NASA/CR—1999–209561

Characterizing Secondary Debris Impact Ejecta

W.P. Schonberg
University of Alabama in Huntsville, Huntsville, Alabama

Prepared for Marshall Space Flight Center
under Contract NAS8–97095
and sponsored by
The Space Environments and Effects Program
managed at the Marshall Space Flight Center

National Aeronautics and
Space Administration

Marshall Space Flight Center • MSFC, Alabama 35812

August 1999

Acknowledgments

The author is grateful for the support provided by the NASA Marshall Space Flight Center that made this study possible. The author would also like to acknowledge Gregory Olsen for his guidance during the course of this effort.

Available from:

NASA Center for AeroSpace Information
800 Elkridge Landing Road
Linthicum Heights, MD 21090–2934
(301) 621–0390

National Technical Information Service
5285 Port Royal Road
Springfield, VA 22161
(703) 487–4650

PREFACE

The effort described in this report was supported by the Structural Development Branch (ED52) of the NASA/Marshall Space Flight Center in Huntsville, Alabama. The Contracting Officer's Technical Representatives for this program was Mr. Gregory Olsen (ED52).

TABLE OF CONTENTS

LIST OF FIGURES

LIST OF TABLES

1.0 INTRODUCTION

All spacecraft in low earth orbit are subject to high speed impacts by meteoroids and orbital debris particles. These impacts can damage flight-critical systems, which can in turn lead to catastrophic failure of the spacecraft. Therefore, the design of a spacecraft for an earth orbiting mission must take into account the possibility of such impacts and their effects on the spacecraft structure and on all of its exposed subsystem components.

In addition to threatening the operation of the spacecraft itself, on-orbit impacts also generate a significant amount of damaging ricochet ejecta particles. These high speed particles can destroy critical external spacecraft subsystems, which in turn also poses a threat to the spacecraft and its inhabitants. Ricochet debris particles also increase the contamination of the orbital environment and, as a result, constitute a threat to other missions into that environment. Since the majority of on-orbit debris impacts are expected to occur at oblique angles, the characterization of ricochet debris created in an orbital debris particle impact is an issue that must be addressed.

This report presents a summary of the work performed towards the development of an empirical model that that characterizes the secondary ejecta created by a high speed impact on a typical aerospace structural surface. The empirical model developed provides the following information as a function of impact parameters (speed, angle, projectile diameter) and target plate geometry (e.g. thickness, etc):

- angles defining the spread of ricochet debris and the trajectory of the ricochet debris cloud center-of-mass;
- average velocity of the ricochet debris cloud material; and,
- velocity and mass of the largest particle(s) in the ricochet debris cloud.

In this report, Chapter 2 presents an overview of the phenomenology associated with oblique hypervelocity impacts on thin plates, and compares them with the processes typically involved in normal (i.e. non-oblique) impacts. Chapter 3 presents a summary of the analysis performed to obtain the spatial distributions of ricochet debris particle impacts. This analysis is used to determine ricochet debris cloud spray and trajectory angles in terms of impact parameters and target plate geometry.

The technique for calculating the average velocity of the ricochet debris cloud is presented in Chapter 4. This method is a based on a model developed previously that characterizes the masses, trajectories, and velocities of the debris clouds created in an oblique high-speed impact [1]. This model employs the three conservation principles, elementary shock physics theory, and fundamental thermodynamic principles to obtain a system of algebraic equations for the various debris cloud masses, trajectories, and velocities. This existing model is modified by incorporating the information presented in Chapter 3 and by reducing its dependence on empirical parameters.

In Chapter 5, relationships for crater diameter and depth are applied to the deepest craters in each ricochet witness plate to "back out" the diameters, masses, and velocities of the ricochet debris cloud particles that created these craters. These calculations are performed using a method similar to that developed in a previous study of ricochet debris particles created in oblique hypervelocity impact [2]. The information obtained is then used to develop empirical relationships that predict the velocity and mass of the largest ricochet debris cloud particle in terms of impact parameters and bumper plate thickness. Results obtained using these relationships are compared with those obtained previously and presented in Reference [2]. Conclusions derived from the work presented herein, as well as recommendations for future activities in this area, are presented and discussed in Chapter 6.

2.0 OVERVIEW OF HYPERVELOCITY IMPACT PHENOMENOLOGY

Consider the normal hypervelocity impact of a projectile on the outer bumper of a multi-wall system as shown in Figure 2.1. Upon impact, shock waves are set up in the projectile and outer bumper materials. The pressures associated with these shocks typically exceed the strengths of the materials by several orders of magnitude. For example, in an 8 km/sec aluminum-on-aluminum impact, the ratio of the impact pressure (116.5 GPa=1.15 MBar) to the strength of the material (310 MPa for aluminum 6061-T6) is approx. 375, or roughly 2.5 orders of magnitude.

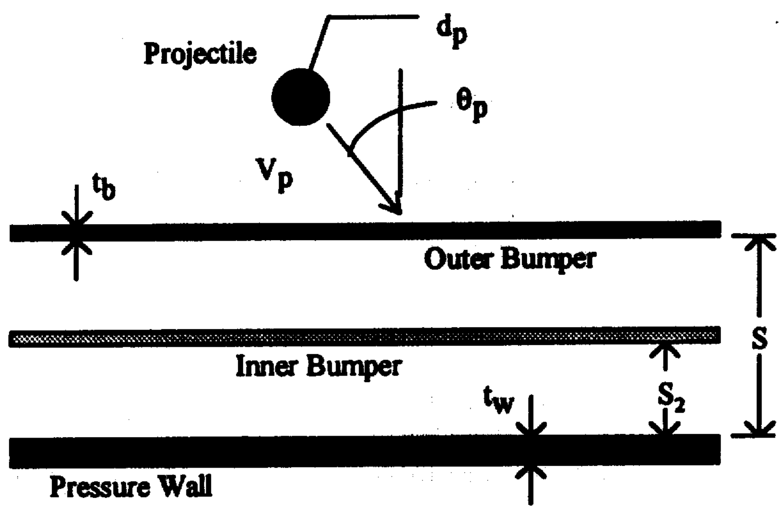

Figure 2.1. Hypervelocity Impact of a Generic Multi-Wall System

As the shock waves propagate, the projectile and outer bumper materials are heated adiabatically and non-isentropically. The release of the shock pressures occurs isentropically through the action of rarefaction waves that are generated as the shock waves interact with the free surfaces of the projectile and the outer bumper. This process leaves the materials in high energy states and can cause either or both to fragment, melt or vaporize, depending on the material properties, geometric parameters, and the velocity of impact.

The outer bumper of the multi-wall structure protects the pressure wall against perforation by disintegrating the impacting particle and by creating one or more diffuse debris clouds. In a normal impact, only one debris cloud containing both projectile and bumper plate fragments is evident. It first strikes the inner bumper and then travels towards and eventually impacts the pressure wall. However, in an oblique impact, three debris clouds are typically formed. Two of them, travel inward towards and eventually strike the pressure wall.

These two debris clouds typically form two distinct areas of damage on the pressure wall. In one damage zone, craters and holes (if any) are nearly circular, which is characteristic of near-normal impact. In the other, the craters (and holes, if any) are oblong, indicating that they are formed by oblique impacts. As a result, these two debris clouds are often referred to as the "normal" and "in-line" debris clouds, respectively. It has hypothesized that the "normal" debris cloud contains mainly bumper plate fragments while the "in-line" debris cloud contains mainly projectile fragments [3].

The third debris cloud, often referred to as the "ricochet" debris cloud, travels backwards, away from the multi-wall system. When the projectile obliquity is 45° or less, only a small quantity of very fine ricochet debris particles are formed. There can be, however, extensive damage to the pressure wall, typically in the form of one or more jagged or petalled holes. As the trajectory obliquity is increased beyond 45°, the amount of ricochet debris produced by the impact increases significantly. Impacts at obliquities beyond 60° or 65° produce a tremendous amount of ricochet debris and only a small quantity of "penetration" debris. The change in behavior that occurs near 60° has led Schonberg [4] to postulate the existence of a "critical angle of impact obliquity". For aluminum projectiles impacting aluminum bumpers, Schonberg estimated the value of this critical angle to be near 60°-65°. Impacts of projectiles with obliquities less than this critical value would result in more damage to the pressure wall than to any exterior spacecraft component, while impacts at obliquities greater than this critical value would result in more damage to external components than to the spacecraft pressure wall.

3.0 RICOCHET DEBRIS CLOUD SPREAD AND TRAJECTORY

In this Chapter, we present a summary of the analyses performed to develop empirical equations that define the in-plane spread and trajectory of the ricochet debris cloud in terms of impact parameters, material properties and bumper thickness. This analysis is based on empirical data from two sources: 1) 225 high speed impact tests performed at the NASA/Marshall Space Flight Center; and, 2) 39 numerical simulation runs performed using SPH, also provided by the NASA/Marshall Space Flight Center.

Figure 3.1 below shows a typical test set-up. This figure is similar to Figure 2.1, except that a "ricochet witness plate" has been added to the diagram. These witness plates were typically 0.3 cm to 1.3 cm thick, depending on the impact conditions, and were provided in each test to capture the ricochet debris particles created by oblique impacts. In Figure 3.1, θ_r and θ_{99} denote the trajectory of the center-of-mass of the fragments in the ricochet debris cloud and the angle below which lies 99% of the damage to the ricochet witness plate, respectively. Based on its definition, θ_{99} is presumed to model the spread of the ricochet debris cloud particles. Post-test examination of damaged ricochet witness plates revealed several interesting characteristics about oblique hypervelocity impact.

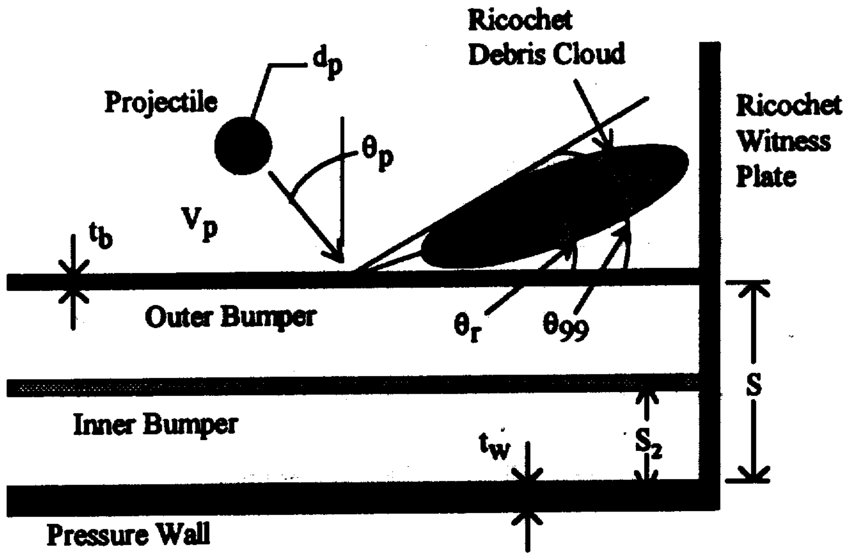

Figure 3.1. Typical Oblique Hypervelocity Impact Test Set-up with Ricochet Debris Cloud

For impact tests in which the obliquity angle was 30° or less, there was virtually no damage to the ricochet witness plate. Under such conditions, only a splash deposition was evident on that plate. As obliquity increased to 45°, the damage to the ricochet witness plate became more pronounced. Small, shallow craters were now evident on the witness plate, typically less than 2 mm in diameter and less than 2 mm deep, and fairly evenly distributed along the height of the witness plate. With further increases in obliquity, an increasing amount of deep cratering became evident on the ricochet witness plates. In fact, if a thin ricochet witness plate (i.e. on the order of 0.3 cm) were used in a test with an obliquity exceeding 65°, it was not unusual to find that the witness plate was perforated along the entire length of the border between it and the outer bumper.

From these observations, it became evident that as impact angle increased, the angle defining the trajectory of the ricochet debris cloud center-of-mass decreased dramatically, that is, as θ_p increased, θ_r decreased. However, even in the high obliquity tests, there were still a fair number of craters near the top of the ricochet witness plates, indicating that as θ_r increased, θ_{99} did not experience any significant changes. Appendix A presents a compilation of the θ_{99} and θ_r data for the oblique impact tests considered in this study. The value of θ_r for each test was obtained by calculating the vertical location of the center of the ricochet witness plate craters using a weighted average technique based on the vertical distribution of the witness plate craters. The angle θ_{99} was determined based on the height below which lay 99% of the ricochet crater damage, and was found simply by counting craters and noting their vertical locations along the witness plate.

To supplement the empirical data, 39 numerical runs were performed using SPH, a smooth particle hydrodynamics code developed for modelling hypervelocity impact phenomena. The impact parameters governing the numerical simulations were chosen to exceed, in terms of projectile diameter and impact velocity, those normally attainable with a light gas gun. In this manner, the "tests" performed using SPH extended the data provided by light gas gun testing. Appendix B presents a compilation of the θ_{99} and θ_r data for the oblique impact tests considered in this study. For the SPH runs, the value of θ_r for each run was obtained by estimating the angle defining the trajectory of the center-of-mass of the ricochet debris cloud based on several SPH output plots. The angle θ_{99} was obtained by estimating the angle below which lay 99% of the ricochet debris cloud particles as shown on the SPH output plots.

Three sets of equations for θ_r and θ_{99} were obtained: 1) an equations for each based solely on empirical data; 2) an equation for each based solely on SPH data; and, 3) an equation for each based on a combined database including both empirical and SPH data. These equations are all in the following form:

$$\tan\theta_{r,99} = A\left(\frac{t_b}{d_p}\right)^B\left(\frac{V_p}{C_b}\right)^C \cos^D\theta_p \qquad (3.1a\text{-}f)$$

where C_b is the bumper material speed of sound.

Table 3.1 below presents the values of the regression coefficients A-D and the correlation coefficients for equations (3.1a-f). Figures 3.2 and 3.3 present a plot of these equations for a 0.795 cm diameter projectile impacting at 0.127 cm thick bumper at a velocity of 6.5 km/s at trajectory obliquities ranging from 45° to 75°. Also shown in these figures are test data and numerical simulation data for θ_r and θ_{99}.

Table 3.1 Parameter Values and Correlation Coefficients for Equations (3.1)

Equation	Quantity	Database	A	B	C	D	Correlation Coefficient (R^2)
3.1a	θ_r	Empirical	0.4725	0.4085	0.2299	0.6458	0.629
3.1b	θ_{99}	Empirical	0.7052	0.2272	0.06828	0.1404	0.343
3.1c	θ_r	SPH	0.1377	-0.5421	0.1028	1.2255	0.837
3.1d	θ_{99}	SPH	1.6519	0.2201	0.1689	1.4587	0.964
3.1e	θ_r	Combined	0.4206	0.2651	0.4345	0.7988	0.662
3.1f	θ_{99}	Combined	0.7608	0.1989	0.1146	0.3191	0.429

As can be seen from Table 3.1, the SPH-only equations have the highest correlation coefficients, indicating that the SPH data is very consistent from run to run. In addition, the empirical-only and combined equations for θ_r have reasonable R^2 values, which indicates that although there is a fair degree of scatter in the empirical θ_r data, the trends in the data are consistent over the range of empirical parameters considered. However, as is apparent from the very low R^2 values for the empirical and combined θ_{99} equations, there are some features in the θ_{99} data that are not accounted for in the regression model selected. Additional discussion of these features follow Figures 3.2 and 3.3 below.

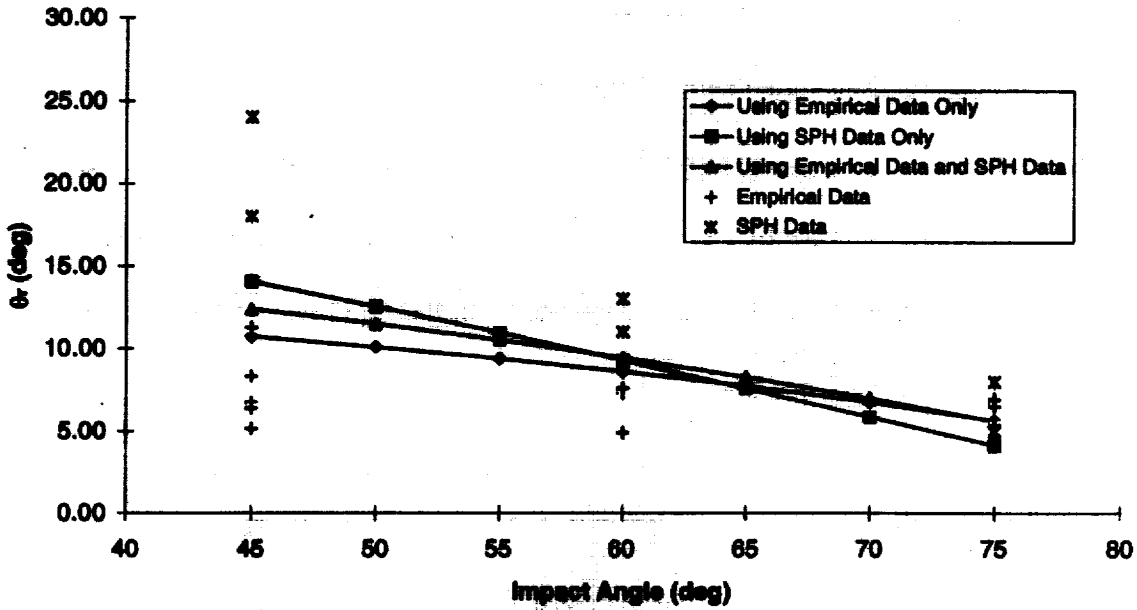

Figure 3.2 Comparison of θ_r Regression Equation Predictions Against Empirical and Numerical Data

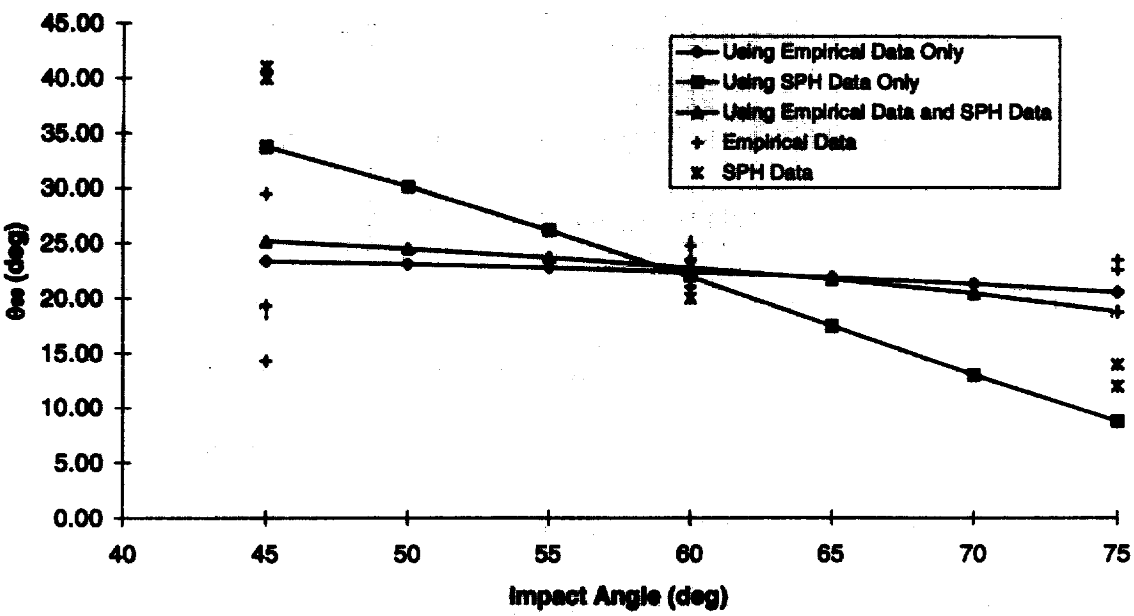

Figure 3.3 Comparison of θ_{99} Regression Equation Predictions Against Empirical and Numerical Data

It is clear from the plots of all three regression equations in Figure 3.2 (empirical-only, SPH-only, and combined) that θ_r decreases monotonically as θ_p increases. This is a statistical demonstration of the empirical observation made previously regarding the nature of the damage to the ricochet witness plates and its relationship to the trajectory obliquity of the impacting projectile.

However, Figure 3.3 shows a divergence in the trend predicted by the SPH-only regression and those predicted by the empirical-only and combined egressions. The SPH data and the associated curve clearly show a dependence of θ_{99} on θ_p, one that is similar to that observed for θ_r: as θ_p increases, θ_{99} decreases. However, the empirical data and the associated curves show θ_{99} to be relatively insensitive to any variation in θ_p. The implication is that the empirical evidence dictates that the majority of the ricochet debris cloud particles will always be contained within the same spread angle (25° in this case), regardless of the impact parameters.

The apparent lack of dependence of θ_{99} on any impact parameter would also explain the low correlation coefficients obtained when regressing the θ_{99} data. A multi-variable regression process seeks to find trends in the data. When there are none, such as in the case of a constant dependent function value, the process returns a correlation coefficient near zero. The discrepancy between the empirically-observed *in*dependence and the numerically-observed dependence of θ_{99} is an issue that needs to be explored in more detail in a subsequent investigation. Perhaps more consistent calculation (in the case of the test data) and measurement (in the case of the numerical data) processes are needed to ensure a more valid joining of the two data sets.

4.0 RICOCHET DEBRIS CLOUD VELOCITY

4.1 Introductory Comments

A model is developed that can be used to calculate the masses, velocitities, and trajectories of the three debris clouds created in an oblique hypervelocity impact in terms of impact parameters, material properties, and bumper thickness. This model is based on applying the principles of mass, momentum, and energy conservation before and after the oblique impact event. Elementary shock physics and thermodynamic principles are used in the model to determine the fraction of the initial projectile impact energy that is lost to shock heating of the projectile and bumper materials. The model developed is verified by comparing its predictions with available experimental information.

The model is an improvement of the original model developed by Schonberg and Yang [1] for two reasons. First, it contains a more widely-applicable empirical equation for θ_r than the previous model. Second, it has a decreased dependence on empirical, or user-controlled, parameters by explicitly calculating the fraction of the initial projectile kinetic energy that is expended in the shock heating and release of the projectile and bumper materials.

Figure 4.1 below shows a schematic of the parameters that characterize the motion of the three debris clouds created in an oblique hypervelocity impact. In this figure, M_1, M_2, and M_r are the masses of the 'normal", 'in-line', and 'ricochet' debris clouds. Analogously, the quantities V_1, V_2 and V_r, and θ_1, θ_2, and θ_r are the axial velocities and trajectories, respectively, of these debris clouds. We also later introduce the parameter V_e (not shown in Figure 4.1) which is used to characterize the (assumed equal) radial expansion velocity of each of these three debris clouds.

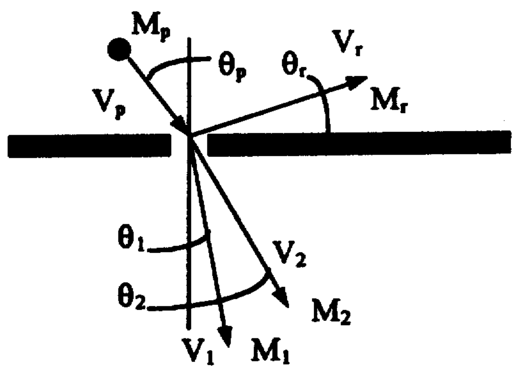

Figure 4.1. Oblique Hypervelocity Impact of a Flat Plate

4.2 Oblique Impact Model Development

Applying conservation of momentum before and after the initial impact of the projectile on the bumper plate in the vertical and horizontal directions, we arrive at the following equations:

$$M_p V_p \cos\theta_p = M_1 V_1 \cos\theta_1 + M_2 V_2 \cos\theta_2 - M_r V_r \sin\theta_r \qquad (4.1)$$

$$M_p V_p \sin\theta_p = M_1 V_1 \sin\theta_1 + M_2 V_2 \sin\theta_2 + M_r V_r \cos\theta_r \qquad (4.2)$$

Assuming that no mass is lost in the initial impact, the mass conservation principle yields

$$M_p + M_f = M_1 + M_2 + M_r \qquad (4.3)$$

where M_f is the mass of the material that is punched out in the creation of the eliptical hole in the bumper plate. This quantity is calculated by noting that for the trajectory obliquities considered, the bumper plate hole is elliptical [5]:

$$M_f = \frac{1}{4}\pi\rho_b D_{min} D_{max} t_b \qquad (4.4)$$

where ρ_b and t_b are the bumper mass density and thickness, respectively.

The quantities D_{min} and D_{max} are the lengths of the minor and major axes of the bumper plate hole and were calculated using the following empirical equations [4]:

$$\frac{D_{min}}{d_p} = 2.698\left(\frac{V_p}{C_b}\right)^{0.689}\left(\frac{t_b}{d_p}\right)^{0.708}\cos^{0.021}\theta_p + 0.93 \tag{4.5}$$

$$\frac{D_{max}}{d_p} = 2.252\left(\frac{V_p}{C_b}\right)^{0.622}\left(\frac{t_b}{d_p}\right)^{0.667}\exp(0.815\theta_p) + 1.00 \tag{4.6}$$

where C_b is the bumper material speed of sound, d_p is the projectile diameter, and θ_p is in radians. We note that these equations were derived from hypervelocity impact tests in which spherical aluminum projectiles impacted thin aluminum plates. Hence, while the general methodology described herein may be valid for other materials besides aluminum, the use of empirical equations based on tests employing aluminum plates renders this specific analysis valid only for spherical aluminum projectiles impacting aluminum bumper plates.

Equations (4.1-4.3) constitute a system of 3 equations in 9 unknowns which must be solved for: 3 debris cloud masses, 3 axial velocities, 3 center-of-mass trajectories. An additional unknown exists in the form of the average radial expansion velocity of the debris clouds V_e, which must also be solved for. The solution process is facilitated by utilizing experimental observations from high-speed impact tests of aluminum dual-wall structures to determine several of the unknowns in equations (4.1-4.3). The remaining unknowns can then be determined in closed form. Once this is accomplished, an additional equation can be introduced to solve for V_e. The process by which this is done is described in the following sections.

4.3 Trajectory Angles

The angles θ_1 and θ_2 initially increase as θ_p is increased [4]. This continues until a critical value of θ_p is reached beyond which θ_1 and θ_2 decrease with continued increases in θ_p. This kind of behavior is very difficult to predict analytically without resorting to an advanced shock physics analysis. As a result, the analytical prediction of this behavior is beyond the scope of the present work. The empirical equations used to calculate values of θ_1 and θ_2 as functions of the initial impact parameters are given below [5]:

$$\frac{\theta_1}{\theta_p} = 0.471\left(\frac{V_p}{C_b}\right)^{-0.049}\left(\frac{t_b}{d_p}\right)^{-0.054}\cos^{1.134}\theta_p \tag{4.7}$$

$$\frac{\theta_2}{\theta_p} = 0.532\left(\frac{V_p}{C_b}\right)^{-0.086}\left(\frac{t_b}{d_p}\right)^{-0.478}\cos^{0.586}\theta_p \tag{4.8}$$

The angle θ_r is given by the following empirical equation, which was derived in the preceding chapter:

$$\theta_r = \tan^{-1}\left[0.4206\left(\frac{t_b}{d_p}\right)^{0.2651}\left(\frac{V_p}{C_b}\right)^{0.4345}\cos^{0.7988}\theta_p\right] \tag{4.9}$$

By using equations (4.7-4.9), θ_1, θ_2, and θ_r can be treated as known quantities which reduces the number of unknowns in equations (4.1-4.3) to six.

4.4 Debris Cloud Masses

The three unknown debris cloud masses are calculated by systematically distributing the mass of the projectile and the mass of the bumper plate material that is punched out by the initial impact among the three debris clouds and then invoking the conservation of mass equation, equation (4.3). This distribution process is accomplished as follows.

First, it is noted that as θ_p increases, the amount of material in the normal and in-line debris clouds monotonically decreases while that in the ricochet debris cloud steadily increases [5]. Furthermore, it has been hypothesized that the material in the normal debris cloud is primarily bumper plate material, while the material in the in-line debris cloud is primarily projectile material [3]. The obliquity of the initial impact on the bumper plate also mandates that the in-line and ricochet debris clouds contain a portion of the bumper plate material. Based on these observations, we postulate the following functional forms of M_1 and M_2:

$$M_1 = \overline{M_f} \cos^n \theta_p \qquad (4.10)$$

$$M_2 = \alpha_2 (M_f - \overline{M_f}) \cos^n \theta_p + M_p \cos^n \theta_p \qquad (4.11)$$

where $\overline{M_f}$ is the mass of bumper plate material that would be ejected in a normal impact at a reduced velocity $V' < V_p$, i.e. $\overline{M_f} = M_f(\theta_p{=}0°, V_p{=}V')$, and α_2 is that fraction of the ejected bumper plate material in the in-line debris cloud. These forms satisfy the requirement that the debris cloud masses decrease as θ_p increases and do not violate the hypotheses regarding the origins of the material in the respective debris clouds. The values of the exponent n and the coefficient α_2 are adjusted so that the final predictions for the debris cloud spread angles based on this analysis procedure compare well with those obtained using empirical predictor equations for debris cloud spread angles.

The reduced velocity V' used to calculate the mass of bumper plate material in the 'normal' debris cloud is taken to be the normal component of the original impact velocity. Any material in excess of that which such a normal impact would produce is allocated to the 'in-line' and ricochet debris clouds. Therefore, the reduced velocity V' is given by

$$V' = \eta V_p \cos\theta_p \qquad (4.12)$$

where η is a correction factor that is also adjusted so that the final predictions for debris cloud spread angles based on the analysis procedure presented herein compare well with those obtained using empirical predictor equations. Substitution of equations (4.10-4.11) into equation (4.3) results in the following expression for the mass of the ricochet debris cloud:

$$M_r = (1 - \alpha_2)(M_f - \overline{M_f}) \cos^n \theta_p + (M_f + M_p)(1 - \cos^n \theta_p) \qquad (4.13)$$

These calculations and assumptions allow M_1, M_2, and M_r to be treated as known quantities which reduces the number of unknowns to three. Since one of the equations was used in the preceding analysis, we now have a system of two equations in three unknowns (V_1,V_2,V_r).

4.5 Debris Cloud Axial Velocities

Since the 'normal' debris cloud is assumed to contain only bumper plate material and the mass of that material is calculated assuming a normal impact, the method for calculating its velocity is based on a procedure currently utilized for calculating debris cloud velocities in normal impacts of thin plates. This procedure is summarized in the following paragraph.

The initial normal impact of a projectile on a thin plate produces a shock wave that undergoes reflection at the rear surface of the plate. An elementary shock wave propagation analysis indicates that the velocity of the rear surface at the moment of reflection is equal to twice the particle velocity of the plate material as the shock wave passes through the plate. For a normal impact of an aluminum projectile on an aluminum plate, particle velocity is equal to one-half of the impact velocity. Hence, a simple substitution shows that for the particular projectile and bumper plate materials under consideration, under normal impact, the velocity of the rear surface of the plate is equal to the initial normal impact velocity. Since the reflection of the shock wave from the rear surface causes the plate material to fragment and thereby creates the debris cloud, the presumption is made that the axial velocity of the debris cloud created by the normal impact is equal to the velocity of the rear surface of the plate.

Since the normal velocity assumed to create the 'normal' debris cloud is given by V', then the axial velocity of the 'normal' debris cloud is also given by V', that is,

$$V_1 = \eta V_p \cos\theta_p \tag{4.14}$$

We are now left with a system of two equations in two unknowns, V_2 and V_r. This system is solved explicitly with the following results:

$$V_2 = \frac{M_p V_p \cos(\theta_p - \theta_r) - V_1 \cos(\theta_1 - \theta_r)}{M_2 \cos(\theta_2 - \theta_r)} \tag{4.15}$$

$$V_r = \frac{M_p V_p \sin\theta_p - M_1 V_1 \sin\theta_1 - M_2 V_2 \sin\theta_2}{M_r \cos\theta_r} \tag{4.16}$$

Thus, all of the unknowns in equations (4.1-4.3) are now determined. The final unknown to be determined is V_e, which is found using the method presented in the next Section. It is necessary to determine this unknown in order to be able to validate this model.

4.6 Debris Cloud Radial Expansion Velocities

If we apply the principle of energy conservation before and after the initial impact of the projectile on the bumper plate, we have the following symbolic equation:

$$K.E_{\text{-initial}} = K.E_{\text{-debris}} + K.E_{\text{-lost}} \tag{4.17}$$

where the initial kinetic energy is that of the incoming projectile, the kinetic energy of the debris clouds is that due to their axial motion and expansion, and the kinetic energy that is lost is due to the irreversible thermodynamic processes that result from the initial impact such as material heating, light flash, etc. If the energy that is lost is written as some fraction ξ of the initial impact energy, then writing the kinetic energy of the projectile and the debris clouds in standard form yields the following:

$$\frac{1}{2}(1-\xi) M_p V_p^2 = \frac{1}{2}(M_1 + M_2 + M_r) V_e^2 + \frac{1}{2}(M_1 V_1^2 + M_2 V_2^2 + M_r V_r^2) \tag{4.18}$$

The term on the left hand side of equation (4.18) may be regarded as the energy available for debris cloud motion and expansion. Once the value of ξ is known, the only unknown in equation (4.18) is V_e, which can be obtained explicitly as follows:

$$V_e = \sqrt{\frac{(1-\xi) M_p V_p^2 - (M_1 V_1^2 + M_2 V_2^2 + M_r V_r^2)}{M_1 + M_2 + M_r}} \tag{4.19}$$

The parameter ξ, which defines the fraction of the initial impact energy that is lost to shock heating, is calculated as follows:

$$\xi = \frac{E_{lost}^{proj} M_p + E_{lost}^{bmpr} M_f}{\frac{1}{2} M_p V_p^2} \tag{4.20}$$

where E_{lost}^{proj} and E_{lost}^{bmpr} are the waste heats per unit mass produced by the shock heating and release of the projectile and bumper hole-out materials. We note that by neglecting energy losses such as those due to light flash, the results obtained herein should be conservative in nature. The procedure for calculating these waste heats is discussed in the following sub-section.

4.6.1 Shock Loading and Release Due to High Speed Impact

In calculating the shock loading and subsequent release of the projectile and outer bumper materials, the shock waves are considered to be initially planar. This simplification allows one-dimensional relationships to be used for analyzing the creation and release of shock pressures. In this manner, the shock pressures, energies, etc., in the projectile and outer bumper materials are calculated using the three 1-D shock-jump conditions, a linear relationship between the shock wave velocity and particle velocity in each material, and continuity of pressure and velocity at the projectile/outer bumper interface. Specifically, if we consider the 1-D impact of a projectile with velocity v_o on a stationary outer bumper, conservation of mass, momentum, and energy across the shock fronts in the projectile and in the outer bumper yields

$$\frac{u_{sp}}{V_{op}} = \frac{u_{sp} - u_{pp}}{V_{Hp}}$$

<u>Projectile</u>: $$P_{Hp} = P_{op} + \frac{u_{sp} u_{pp}}{V_{op}} \qquad (4.21a\text{-}c)$$

$$E_{Hp} = E_{op} + \frac{1}{2}(P_{Hp} + P_{op})(V_{op} - V_{Hp})$$

$$\frac{u_{st}}{V_{ot}} = \frac{u_{st} - u_{pt}}{V_{Ht}}$$

<u>Outer Bumper</u>: $$P_{Ht} = P_{ot} + \frac{u_{st} u_{pt}}{V_{ot}} \qquad (4.22a\text{-}c)$$

$$E_{Ht} = E_{ot} + \frac{1}{2}(P_{Ht} + P_{ot})(V_{ot} - V_{Ht})$$

where $V=1/\rho$ is specific volume, u_s and u_p are shock and particle velocity, respectively; V_H, P_H, E_H and V_o, P_o, E_o are the density, pressure and energy states associated with the shocked and initial material states, respectively. In equations (4.21a-c) and (4.22a-c), the subscripts 'p', and 't' refer to projectile and outer bumper quantities, respectively. In the development of equations (4.21a-c) and (4.22a-c), the shock velocity in the projectile is taken relative to a 'stationary' projectile.

The linear shock velocity-particle velocity relationships for the projectile and outer bumper materials are taken to be in the form

$$u_s = c_o + ku_p \qquad (4.23)$$

where $c_o=\sqrt{(KV_o)}$ is the material bulk speed of sound, $K=E/3(1-2v)$ is the adiabatic bulk modulus, E and ν are Young's modulus and Poisson's ratio, respectively, and k is an empirically-derived constant. Equations (4.21a-c, 4.22a-c) are applied to the initial impact on the outer bumper of a multi-wall system in the following manner. Upon impact, pressure equilibrium at the projectile/outer bumper interface implies that

$$P_{Hp} = P_{Ht} \qquad (4.24)$$

while material continuity at the interface implies that

$$v_o = u_{pp} + u_{pt} \tag{4.25}$$

Because the outer bumper in a multi-wall system is free from any initial mechanical stress (it is merely supported at its four corners a fixed distance away from the inner pressure wall), the initial conditions ahead of the projectile and outer bumper shock waves are taken to be zero (with the exception, of course, of the initial material densities). Solving equations (4.21-4.25) simultaneously yields expressions for projectile and outer bumper particle velocities which can then be used to calculate shock velocities, pressures, internal energies, and material densities after the passage of a shock wave. For example, using this procedure to solve initially for u_{pt} yields

$$u_{pt} = \frac{b - \sqrt{\Delta}}{2a} \tag{4.26}$$

where

$$\begin{aligned} a &= k_p - k_t\left(\frac{\rho_{ot}}{\rho_{op}}\right) \\ b &= 2k_p v_o + c_{op} + c_{ot}\left(\frac{\rho_{ot}}{\rho_{op}}\right) \\ \Delta &= b^2 - 4a(c_{op}v_o + k_p v_o^2) \end{aligned} \tag{4.27a-c}$$

Then it follows that

$$\begin{aligned} u_{pp} &= v_o - u_{pt} \\ u_{st} &= c_{ot} + k_t u_{pt} \\ u_{sp} &= c_{op} + k_p u_{pp} \end{aligned} \tag{4.28a-c}$$

The shocked densities of the projectile and outer bumper materials are found by substituting equations (4.26, 4.28a-c) into equations (4.21a) and (4.22a) to yield

$$\rho_{Hp} = \frac{1}{V_{Hp}} = \frac{u_{sp} / V_{op}}{u_{sp} - u_{pp}} \tag{4.29a}$$

$$\rho_{Ht} = \frac{1}{V_{Ht}} = \frac{u_{st} / V_{ot}}{u_{st} - u_{pt}} \tag{4.29b}$$

Finally, equations (4.21b,c) and (4.22b,c) are then used to define the pressure and energy in the projectile and outer bumper materials, respectively, associated with the passage of the shock waves created by the initial impact. This completely defines the shocked states of the projectile and outer materials due to the initial impact.

While the shock loading of a material is an irreversible process that results in an increase of the internal energy of the shocked material, the release of a shocked material occurs isentropically along an 'isentrope' or 'release adiabat'. The difference between the area under the isentrope and the energy of the shocked state is the amount of residual energy that remains in the material and can cause the material to melt or even vaporize. In order to calculate the release of the projectile and outer bumper materials from their respective shocked states (each characterized by P_H, E_H, and V_H), an appropriate equation-of-state is needed for each material. To keep the analysis relatively simple, the Mie-Gruneisen equation-of-state [6] was used in this study.

The Mie-Gruneisen equation-of-state (EOS) is an accurate thermodynamic description of most metals in the solid regime and is relatively easy to use. It has the form

$$P = P_H + \rho\Gamma(E - E_H) \tag{4.30}$$

where the time-dependent Gruneisen coefficient Γ is given for most metals as

$$\Gamma = \frac{\Gamma_o \rho_o}{\rho} \tag{4.31}$$

In equation (4.31),

$$\Gamma_o = \frac{K\beta}{\rho_o C_p} \tag{4.32}$$

is the ambient Gruneisen coefficient, where K is the adiabatic bulk modulus, $\beta=3\alpha$ is the volumetric coefficient of thermal expansion, and C_p is specific heat at constant pressure. Invoking the Second Law of Thermodynamics

$$dE = TdS - PdV \tag{4.33}$$

along with the isentropic constraint dS=0 for the release process allows us to construct the release isentrope in P-V space for a material referenced to the material Hugoniot in P-V space and a given initial shocked state defined by P_H, V_H, E_H. Using the procedure outlined in Reference [6], the pressure P_i at a specific position 'i' along the isentrope can be shown to be given by

$$P_i = \frac{P_{Hi} + \left(\frac{\Gamma}{V}\right)_i \left(E_{i-1} - \frac{1}{2}P_{i-1}(\Delta V) - E_{Hi}\right)}{1 + \frac{1}{2}\left(\frac{\Gamma}{V}\right)_i (\Delta V)} \tag{4.34}$$

where ΔV is the incremental change in volume used to create the release isentrope, and P_{Hi} and E_{Hi} are the pressure and energy along the Hugoniot corresponding to the i-th position in the release process. The release process is continued using equation (4.34) until the release isentrope so determined crosses the V-axis.

It should be noted that based on its formulation, the Mie-Gruneisen EOS cannot be expected to give accurate results in a highly expanded liquid regime or in a vapor regime. This is because as impact energy increases, the assumption that the Gruneisen coefficient is a function of density alone is no longer valid. At high impact energies, the Gruneisen coefficient is a function of internal energy as well as density. Experience has shown, however, that it does yield fairly accurate end-state results even when there is a small percentage of molten material present [7].

Once the release process calculations for the projectile and bumper materials have been completed, the areas under the respective isentropes are calculated and subtracted from the initial shocked energy state to determine the respective waste heats, that is,

$$E_{lost}^{proj} = E_H - A_{isen}^{proj} \tag{4.35a}$$

$$E_{lost}^{bmpr} = E_H - A_{isen}^{bmpr} \tag{4.35b}$$

4.7 Oblique Impact Model Verification

The validity of the proposed method of solution for the ten unknowns that characterize the debris clouds created as a result of an oblique hypervelocity impact of a thin plate (as well as all the attendant assumptions) is assessed by comparing model predictions of debris cloud spread angles with the predictions of empirically based equations for debris cloud spread angles. Model values for the spread angles of the 'normal' and 'in-line' debris clouds, ϕ_1 and ϕ_2, respectively, are given by:

$$\phi_i = 2\tan^{-1}\left(\frac{V_e}{V_i}\right) \qquad i = 1, 2 \tag{4.36}$$

The empirical values of debris cloud spread angles are found using the following relationships [5]:

$$\tan\phi_1 = 1.318\left(\frac{V_p}{C_b}\right)^{0.907}\left(\frac{t_b}{d_p}\right)^{0.195} \cos^{0.394}\theta_p \tag{4.37a}$$

$$\tan\phi_2 = 1.556\left(\frac{V_p}{C_b}\right)^{1.906}\left(\frac{t_b}{d_p}\right)^{0.345} \cos^{0.738}\theta_p \tag{4.37b}$$

Table 4.1 presents the a summary of the impact paramters used in the evaluation of the model developed herein. Tables 4.2a-c, 4.3a-c, and 4.4a-c present the final values of the user-controlled parameters α_2, η and n corresponding to the impact conditions in Table 4.1.

Table 4.1. Impact Conditions Considered in Model Validation

Impact Parameter	Values Considered
Impact Velocity, V_p (km/s)	4.0, 5.5, 7.0
Trajectory Obliquity, θ_p (deg)	30, 45, 60
Projectile Diameter, d_p (cm)	0.635, 0.795, 0.953, 1.13, 1.27
Bumper Thickness, t_b (mm)	1.3, 1.6, 2.0

Table 4.2a. Model Parameters α_2, η and n for θ_p=30°, t_b=1.3 mm

V (km/s)	d_p (cm)	η	N	α_2
4.0	0.635	0.85	3.45	1.00
4.0	0.795	1.00	2.40	1.00
4.0	0.953	1.20	1.50	1.00
4.0	1.13	1.35	0.35	1.00
5.5	0.635	0.80	3.45	1.00
5.5	0.795	0.85	2.45	1.00
5.5	0.953	1.00	1.40	1.00
5.5	1.13	1.20	0.60	1.00
7.0	0.635	0.75	3.40	0.95
7.0	0.795	0.80	2.50	0.93
7.0	0.953	0.90	1.50	0.91
7.0	1.13	1.10	0.90	0.89

Table 4.2b. Model Parameters α_2, η and n for θ_p=30°, t_b=1.6 mm

V (km/s)	d_p (cm)	η	n	α_2
4.0	0.635	0.85	4.50	1.00
4.0	0.795	0.95	3.40	1.00
4.0	0.953	1.05	2.50	1.00
4.0	1.13	1.15	1.60	1.00
5.5	0.635	0.75	4.50	1.00
5.5	0.795	0.85	3.45	1.00
5.5	0.953	0.95	2.60	1.00
5.5	1.13	1.05	1.80	1.00
7.0	0.635	0.75	4.40	0.95
7.0	0.795	0.80	3.50	0.93
7.0	0.953	0.85	2.70	0.91
7.0	1.13	0.90	1.90	0.89

Table 4.2c. Model Parameters α_2, η, and n for θ_p=30°, t_b=2.0 mm

V (km/s)	d_p (cm)	η	n	α_2
4.0	0.635	0.80	5.70	1.00
4.0	0.795	0.90	4.50	1.00
4.0	0.953	1.00	3.60	1.00
4.0	1.13	1.10	2.80	1.00
5.5	0.635	0.75	5.70	1.00
5.5	0.795	0.80	4.45	1.00
5.5	0.953	0.85	3.55	1.00
5.5	1.13	0.90	2.75	1.00
7.0	0.635	0.70	5.50	0.95
7.0	0.795	0.75	4.30	0.93
7.0	0.953	0.80	3.50	0.91
7.0	1.13	0.85	2.70	0.89

Table 4.3a. Model Parameters α_2, η, and n for θ_p=45°, t_b=1.3 mm

V (km/s)	d_p (cm)	η	n	α_2
4.0	0.635	1.00	1.85	1.00
4.0	0.795	1.10	1.35	1.00
4.0	0.953	1.35	0.85	1.00
4.0	1.13	1.50	0.40	1.00
5.5	0.635	0.95	1.95	1.00
5.5	0.795	1.05	1.35	1.00
5.5	0.953	1.10	0.85	1.00
5.5	1.13	1.15	0.28	1.00
7.0	0.635	0.85	1.85	0.95
7.0	0.795	0.95	1.35	0.93
7.0	0.953	1.05	0.90	0.91
7.0	1.13	1.15	0.45	0.89

Table 4.3b. Model Parameters α_2, η, and n for θ_p=45°, t_b=1.6 mm

V (km/s)	d_p (cm)	η	n	α_2
4.0	0.635	1.00	2.45	1.00
4.0	0.795	1.10	1.90	1.00
4.0	0.953	1.20	1.40	1.00
4.0	1.13	1.35	1.00	1.00
5.5	0.635	0.95	2.55	1.00
5.5	0.795	1.05	1.95	1.00
5.5	0.953	1.10	1.45	1.00
5.5	1.13	1.15	1.05	1.00
7.0	0.635	0.85	2.45	0.95
7.0	0.795	0.95	1.90	0.93
7.0	0.953	1.05	1.45	0.91
7.0	1.13	1.15	1.05	0.89

Table 4.3c. Model Parameters α_2, η, and n for θ_p=45°, t_b=2.0 mm

V (km/s)	d_p (cm)	η	n	α_2
4.0	0.635	1.00	3.05	1.00
4.0	0.795	1.10	2.50	1.00
4.0	0.953	1.20	2.00	1.00
4.0	1.13	1.35	1.60	1.00
5.5	0.635	0.95	3.05	1.00
5.5	0.795	1.05	2.45	1.00
5.5	0.953	1.10	2:00	1.00
5.5	1.13	1.15	1.65	1.00
7.0	0.635	0.80	2.85	0.95
7.0	0.795	0.90	2.40	0.93
7.0	0.953	1.00	1.95	0.91
7.0	1.13	1.10	1.65	0.89

Table 4.4a. Model Parameters α_2, η, and n for θ_p=60°, t_b=1.3 mm

V (km/s)	d_p (cm)	η	n	α_2
4.0	0.635	1.50	1.55	1.00
4.0	0.795	1.60	1.20	1.00
4.0	0.953	1.70	0.90	1.00
4.0	1.13	1.80	0.65	1.00
5.5	0.635	1.40	1.55	1.00
5.5	0.795	1.50	1.25	1.00
5.5	0.953	1.60	0.95	1.00
5.5	1.13	1.70	0.70	1.00
7.0	0.635	1.30	1.55	0.95
7.0	0.795	1.40	1.25	0.93
7.0	0.953	1.50	0.95	0.91
7.0	1.13	1.60	0.70	0.89

Table 4.4b. Model Parameters α_2, η and n for θ_p=60°, t_b=1.6 mm

V (km/s)	d_p (cm)	η	n	α_2
4.0	0.635	1.50	1.90	1.00
4.0	0.795	1.50	1.50	1.00
4.0	0.953	1.55	1.20	1.00
4.0	1.13	1.75	1.00	1.00
5.5	0.635	1.40	1.90	1.00
5.5	0.795	1.50	1.60	1.00
5.5	0.953	1.60	1.30	1.00
5.5	1.13	1.70	1.05	1.00
7.0	0.635	1.30	1.85	0.95
7.0	0.795	1.40	1.55	0.93
7.0	0.953	1.50	1.25	0.91
7.0	1.13	1.60	1.00	0.89

Table 4.4c. Model Parameters α_2, η and n for θ_p=60°, t_b=2.0 mm

V (km/s)	d_p (cm)	η	n	α_2
4.0	0.635	1.50	2.25	1.00
4.0	0.795	1.50	1.90	1.00
4.0	0.953	1.55	1.60	1.00
4.0	1.13	1.75	1.35	1.00
5.5	0.635	1.30	2.20	1.00
5.5	0.795	1.40	1.90	1.00
5.5	0.953	1.50	1.60	1.00
5.5	1.13	1.60	1.40	1.00
7.0	0.635	1.15	2.10	0.95
7.0	0.795	1.25	1.80	0.93
7.0	0.953	1.35	1.60	0.91
7.0	1.13	1.45	1.40	0.89

Finally, Table 4.5a-c present percent error summaries showing differences between prediction and experiment for the various bumper plate thicknesses, impact trajectories, projectile diameters, and obliquities considered. For each perforating debris cloud spread angle, the value shown is the precent difference between model prediction and empirical equation prediction. As can be seen from Table 4.5a-c, the values of the spread angles that result from the calculations described herein are very close to the experimental values. Naturally, the values of the parameters α_2, η and n have been adjusted to ensure that model predictions and empirical results are closely matched.

Table 4.5a. Percent Error Summaries for t_b = 1.3 mm

V_s = 4.0 km/s						
d_p	30 deg		45 deg		60 deg	
(cm)	ϕ_1	ϕ_2	ϕ_1	ϕ_2	ϕ_1	ϕ_2
0.635	0.35	1.81	8.55	8.92	-1.16	0.64
0.795	-11.76	11.01	-8.00	1.42	-9.23	3.48
0.953	-28.10	22.52	-14.62	32.70	-11.00	16.24
1.13	-32.89	55.16	-21.37	51.30	-18.35	19.79
V_s = 5.5 km/s						
d_p	30 deg		45 deg		60 deg	
(cm)	ϕ_1	ϕ_2	ϕ_1	ϕ_2	ϕ_1	ϕ_2
0.635	1.19	4.42	4.51	4.25	4.59	8.05
0.795	-2.44	2.52	-0.52	10.62	-5.77	3.41
0.953	-7.63	25.38	-5.21	26.38	-7.89	14.63
1.13	-22.26	37.46	5.30	65.27	-13.44	20.57
V_s = 7.0 km/s						
d_p	30 deg		45 deg		60 deg	
(cm)	ϕ_1	ϕ_2	ϕ_1	ϕ_2	ϕ_1	ϕ_2
0.635	-0.30	3.63	8.57	6.22	2.09	3.79
0.795	-4.20	-3.27	2.11	4.94	-3.81	-1.01
0.953	-6.95	10.12	-2.69	11.45	-5.62	8.05
1.13	-26.23	14.18	-4.24	26.97	-9.86	14.57

Table 4.5b. Percent Error Summaries for t_b = 1.6 mm

V_p = 4.0 km/s						
d_p (cm)	30 deg		45 deg		60 deg	
	ϕ_1	ϕ_2	ϕ_1	ϕ_2	ϕ_1	ϕ_2
0.635	-1.30	4.97	1.83	2.20	-3.59	-3.72
0.795	-9.38	7.50	-7.50	1.26	4.43	9.00
0.953	-15.55	15.73	-8.33	16.09	4.96	18.93
1.13	-17.19	35.45	-16.88	27.99	-15.71	11.89
V_p = 5.5 km/s						
d_p (cm)	30 deg		45 deg		60 deg	
	ϕ_1	ϕ_2	ϕ_1	ϕ_2	ϕ_1	ϕ_2
0.635	1.23	3.83	-3.15	0.62	-2.16	1.74
0.795	-5.85	3.79	-8.65	3.54	-4.79	0.18
0.953	-13.02	7.67	-6.42	13.20	-5.48	9.39
1.13	-18.37	16.95	-9.89	20.85	-13.71	12.97
V_p = 7.0 km/s						
d_p (cm)	30 deg		45 deg		60 deg	
	ϕ_1	ϕ_2	ϕ_1	ϕ_2	ϕ_1	ϕ_2
0.635	-8.26	9.55	-2.56	1.72	-5.71	5.12
0.795	-9.06	-1.28	-4.63	2.66	-5.92	1.94
0.953	-11.65	-3.94	-8.89	6.60	-6.00	10.71
1.13	-12.07	1.43	-13.33	13.38	-8.95	17.75

Table 4.5c. Percent Error Summaries for t_b = 2.0 mm

V_p = 4.0 km/s						
d_p (cm)	30 deg		45 deg		60 deg	
	ϕ_1	ϕ_2	ϕ_1	ϕ_2	ϕ_1	ϕ_2
0.635	-0.89	5.74	-7.35	5.92	-5.54	-0.85
0.795	-6.74	8.65	-9.07	2.55	-4.10	-4.50
0.953	-15.04	11.36	-11.24	11.53	-4.19	0.96
1.13	-16.07	16.74	-23.04	18.12	-10.27	15.35
V_p = 5.5 km/s						
d_p (cm)	30 deg		45 deg		60 deg	
	ϕ_1	ϕ_2	ϕ_1	ϕ_2	ϕ_1	ϕ_2
0.635	-8.76	9.13	-8.79	8.85	-4.58	3.79
0.795	-4.12	9.67	-9.10	11.77	-2.40	1.18
0.953	-4.48	9.55	-10.13	13.93	-0.93	9.91
1.13	-4.96	14.05	-15.89	13.79	-9.50	10.00
V_p = 7.0 km/s						
d_p (cm)	30 deg		45 deg		60 deg	
	ϕ_1	ϕ_2	ϕ_1	ϕ_2	ϕ_1	ϕ_2
0.635	-14.14	14.05	-7.02	13.81	-6.88	7.85
0.795	-7.69	11.44	-6.78	7.39	-0.49	8.47
0.953	-7.80	6.33	-9.77	10.24	-4.13	0.19
1.13	-7.95	9.03	-16.63	5.31	-9.58	-3.26

5.0 CHARACTERIZING RICOCHET DEBRIS CLOUD PARTICLES

Damage potential estimates of ricochet debris particles created in an oblique hypervelocity impact will contribute significantly to the successful design of an effective protection systems for external spacecraft components and will assist in determining the overall survivability probability of a spacecraft following such an impact. A simple way of modelling the damage potential of a ricochet debris particle is through its size and speed.

In this Chapter, a technique is presented for developing empirical relationships that predict the velocity and mass of the largest ricochet debris cloud particle in terms of impact parameters and bumper plate thickness. This is accomplished by "backing out" the diameters, masses, and velocities of the ricochet debris cloud particles from measured craters penetration depths and surface diameters on the ricochet witness plates of 139 oblique impact tests performed at the NASA/Marshall Space Flight Center. Measured values of crater depth and diameter are used together with empirical relationships for these quantities to determine particle diameters and velocities. Results obtained using these relationships are compared with those obtained previously and presented in Reference [2]. Visual inspection of damaged ricochet witness plates reveal several interesting features that address the validity of this method.

1) The surface openings of ricochet witness plate craters formed by debris impacts were very nearly circular, which is indicative of near-normal impact trajectories. This observation is confirmed by the analysis performed in the preceding chapter, which concluded that most of the ricochet debris particles will be contained within a cone having an apex angle of 30o or less, regardless of the original impact angle.

2) In the tests where the ricochet witness plates were sufficiently thick, the reverse sides of the plates remained smooth and undamaged even though the front sides exhibited significant crater damage. In these cases, the post-impact appearance of the ricochet witness plate was identical to that of a "thick plate" subjected to the same debris particle impact loading.

Based on these observations, the use of thick plate equations for penetration depth and crater diameter due to normal hypervelocity impact is justified provided that the reverse side of the ricochet witness plate in which the crater depths are measured is smooth and undamaged (i.e., no spall or dimpling).

Examination of existing penetration depth equations revealed a strong coupling between particle size and velocity effects. That is, the same size crater can be produced by a small particle traveling at a high speed or by a larger particle traveling at a slower speed. Therefore, in order to have a unique solution for particle size and speed, a second set of equations describing another measurable crater quantity was needed. A search of existing literature on cratering phenomena in hypervelocity impact suggested crater volume to be such a quantity. Thus, a crater volume equation used in conjunction with an equation for penetration depth could be used to solve uniquely for particle size and speed. Since it is more facile to measure the surface diameter of an impact crater than it is to determine its exact volume, the crater volume equations were rewritten in terms of surface diameter. The analysis then proceeded as follows.

First, penetration depths and surface diameters of the three largest craters on ricochet witness plates with undamaged rear surfaces were measured (plates with through-holes or only splash damage were not considered). Second, crater volumes were calculated for each measured crater. The crater with the largest volume, deemed the most damage as a result, was identified and retained for future analysis. By considering only the most damaging crater, the diameters and velocities subsequently calculated would represent upper bounds on ricochet debris sizes and speeds. Measured crater depths and diameters, as well as calculated crater volumes, for each of the 139 ricochet witness plates considered herein are presented in Appendix C.

In the last phase of the analysis, equations for penetration depth and crater diameter were solved for particle diameter and velocity in terms of all other parameters, such as density, yield strength, wave speed, and so forth. Substitution of the appropriate parameter values in these equations yielded an estimate for the size and speed of the particle that produced a particular crater. This procedure was applied to the most damaging crater dimensions as identified previously. The penetration depth and crater mouth diameter equations are listed in Appendix D, some rewritten for consistency. The material property values used in these equations is presented in Table 5.1 below.

Table 5.1 Material Property Values

Symbol	Property	Value	Units
C_b	Bumper Speed of Sound	5.04	km/s
ρ_p	Projectile Density	2.718	gm/cm^3
ρ_b	Bumper Density	2.718	gm/cm^3
H_b	Brinell Hardness Number	130	kg/mm^2
S_b	Bumper Dynamic Hardness	6.37E+10	$dynes/cm^2$
S	Bumper Shear Strength	2.83E+09	$dynes/cm^2$
S_{yb}	Bumper Dynamic Yield Strength	1.85E+10	$dynes/cm^2$
Y_b	Bumper Dynamic Shear Strength	2.78E+09	$dynes/cm^2$
B_b	Bumper Hardness	1.27E+10	$dynes/cm^2$
E_b	Bumper Elastic Modulus	73.8	GPa

Since there are 12 penetration depth equations and 6 crater diameter equations, this method should have resulted in 72 estimates for the diameter and 72 estimates for the velocity of each crater-producing projectile. However, equations (D.11) and (D.12) were not used in subsequent analyses because the upper limit of the velocity regime for which they are valid is much lower than that of the other penetration depth equations. Additionally, in the process of pairing the penetration depth and crater diameter equations, it became evident that not all equation pairs were compatible. Because of the exponential form of the equations, certain combinations of equations led to powers of zero for an unknown diameter or velocity. These particular equation pairs, therefore, could not be used to solve for the unknown quantities. This situation is analogous to finding the intersection of two parallel lines in Euclidean geometry. Specifically, penetration depth equations with a $V^{2/3}$ term could not be paired with crater diameter equations having a V^2 term. Thus, in order to obtain unique solutions for particle velocity and diameter, depth equations *with* a $V^{2/3}$ term could only have been paired against diameter equations *without* a V^2 term, while depth equations *without* a $V^{2/3}$ term were paired against diameter equations *with* a V^2 term.

Furthermore, even though an equation pair did produce a solution, the resultant particle size occasionally exceeded that of the crater diameter, sometimes by a factor of three or four. However, it was previously shown that the heated material surrounding a high-speed impact crater relaxes as it cools after the impact event, which can cause a reduction in crater diameter and depth of approximately 20-25%. Therefore, while it is possible that a crater could have been produced by a particle whose diameter exceeded the size of the crater opening, it is unlikely that the diameter of the particle could have exceeded the surface diameter of the crater it produced by more than 25%. As a result, a particle diameter value greater than 1.25 times a corresponding measured crater surface diameter was rejected.

Figures 5.1 and 5.2 show plots of equations (D.1-D.10), the penetration depth equations, and (D.13-D.18), the crater mouth diameter equations, as a function of impact velocity for the material parameter values given in Table 5.1. Examination of these plots reveals several interesting characteristics of the crater depth and diameter equations.

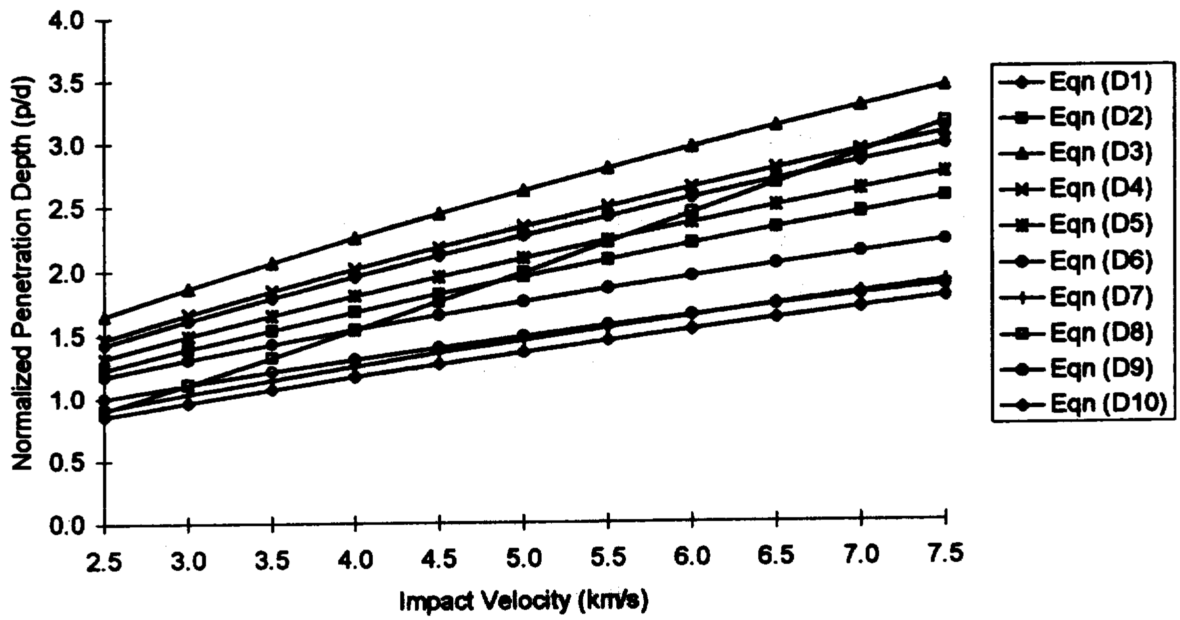

Figure 5.1 Penetration Depth Equations (D.1-D10)

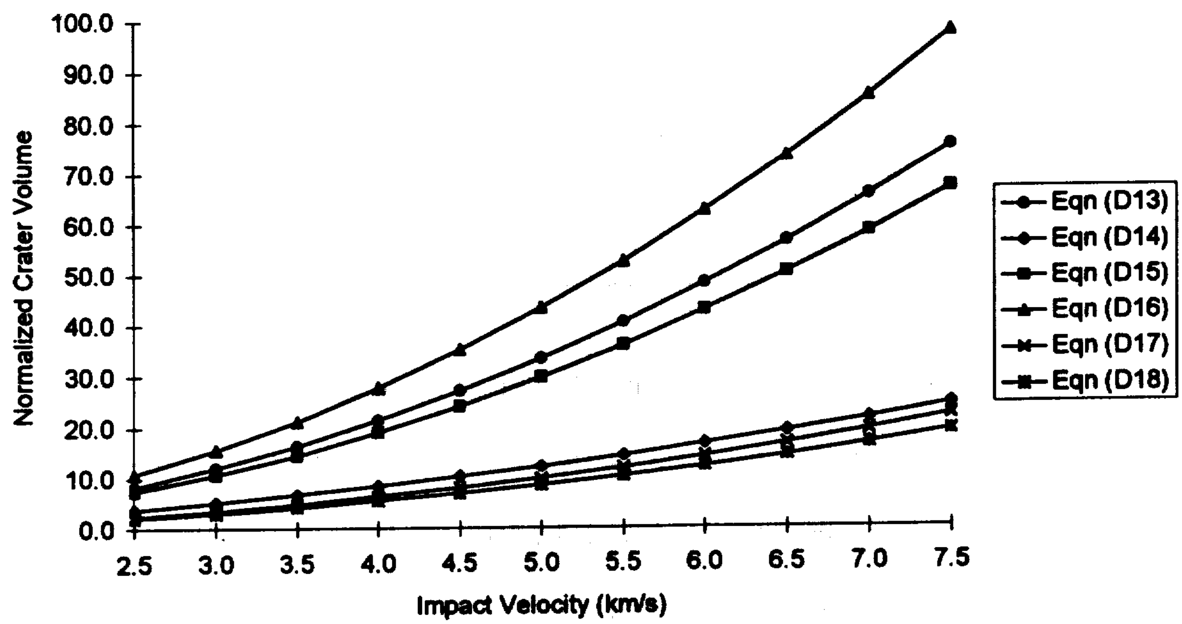

Figure 5.2 Crater Diameter Equations (D.13-D18)

1) With the exception of equation (D.8), all the penetration depth equations are fairly consistent in their prediction trends. The actually values, however, can vary significantly. Because of a lack of corroborative information for the trends and values predicted by equation (D.8), it was not considered in any of the subsequent analyses.

2) The crater equations appear to fall into two fairly distinct groups with regard to both predictive trends as well as predicted values. Within each group, however, the predicted values are fairly consistent.

Based on these observations and the comments made previously regarding the pairing requirements of the depth and diameter equations, the following depth and diameter equation combinations were used to calculate candidate ricochet particle velocity-diameter values:

Table 5.2 Penetration Depth-Crater Diameter Equation Pairs

Penetration Depth Equation No.	Velocity Term	Crater Diameter Equation No.	Velocity Term
D.1	$V^{2/3}$	D.14	$V^{1.69}$
D.2	$V^{2/3}$	D.14	$V^{1.69}$
D.3	$V^{2/3}$	D.14	$V^{1.69}$
D.4	$V^{2/3}$	D.14	$V^{1.69}$
D.5	$V^{2/3}$	D.14	$V^{1.69}$
D.7	$V^{2/3}$	D.14	$V^{1.69}$
D.10	$V^{2/3}$	D.14	$V^{1.69}$
D.6	$V^{0.576}$	D.13	$V^{2/3}$
D.9	$V^{0.576}$	D.13	$V^{2/3}$

These considerations reduced the number of calculated ricochet particle velocity and diameter value pairs for each most damaging crater from 72 to 9 or less. The resulting calculated particle diameters and velocities corresponding to the depths and diameters of the most damaging craters (taken from Appendix D) are given in Appendix E. In Appendix E, 'Vx-y' and 'dx-y' refer to the a particle velocity or diameter, respectively, calculated using a combination of crater depth equation (D.x) and crater mouth diameter (D.y) from Appendix D. Grayed-out areas are calculated particle velocity-diameter combinations that are not valid, most likely because the calculated ricochet particle diameter exceeded the crater mouth diameter (indicated by a value of 'dx-y/d' that is greater than one.

For each test, valid particle velocity-diameter were reviewed to determine two max-min combinations for subsequent regression analyses: V_{max} and the corresponding d_{min}, and V_{min} and the corresponding d_{max}. In this manner, upper and lower bounds on velocity and size can be formed for the most damaging ricochet debris particle to be created in a given impact scenario. These max-min values are provided in Appendix F.

Four empirical predictor equations for were developed using the data in Appendix F. These equations can be used to calculate V_{max}, d_{min}, V_{min}, and d_{max} in terms of bumper thickness and impact parameters, and were all in the following form:

$$\frac{V_i}{V_p} = A\left(\frac{V_p}{C_b}\right)^B \left(\frac{t_b}{d_p}\right)^C \cos^D \theta_p + E \quad , i = \text{max, min} \qquad (5.1a,b)$$

$$\frac{d_i}{d_p} = A\left(\frac{V_p}{C_b}\right)^B \left(\frac{t_b}{d_p}\right)^C \cos^D \theta_p + E \quad , i = \text{max, min} \qquad (5.2a,b)$$

Table 5.3 below presents the values of the regression coefficients A-E and the correlation coefficients for equations (5.1a,b) and (5.2a,b).

Table 5.3 Parameter Values and Correlation Coefficients for Equations (5.1) and (5.2)

Equation	Quantity	A	B	C	D	E	Correlation Coefficient (R^2)
5.1a	V_{max}	0.4294	-1.8335	-0.2799	-0.2562	0.3384	0.417
5.1b	d_{min}	-0.6799	-0.08769	0.01119	1.0558	0.5998	0.712
5.2a	V_{min}	0.3339	-1.2209	-0.1002	-0.1588	0.2206	0.254
5.2b	d_{max}	0.5732	-0.02872	-0.04935	-0.4569	-0.4978	0.747

As can be seen from Table 5.1, the equations for d_{max} and d_{min} have reasonable R^2 values while those for d_{max} and d_{min} are somewhat low. This indicates that there is a fair degree of scatter in the calculated ricochet particle velocity values, while the level of consistency in the calculated diameter values is fairly high. It is not clear at this time why this has occurred, especially since both velocity and diameter quantities were calculated simultaneously using the same data and the same equations.

Equation (5.1a,b) and (5.2a,b) can be used to obtain a bound on the velocity and diameter of the most damaging ricochet debris particle that would be created in a given oblique hypervelocity impact event. However, these equations must be paired appropriately: V_{max} must be paired with d_{min}, while V_{min} must be paired with d_{max}. This will provide, for example, upper and lower limits of expected ricochet particle velocity and the particle diameters corresponding to those velocities.

Figures 5.3 through 5.6 below show plots of equations (5.1a,b) and (5.2a,b) for an initial projectile diameter of 0.795 cm, a 0.127 bumper thickness, for impact velocities ranging between 3 and 8 km/s, and for initial trajectory obliquities of 30°, 45°, 60°, and 75°. In these plots, the open tick marks represent values calculated using equations (51a,b) and (52a,b), while the solid tick marks represent simple numerical averages of corresponding calculated values.

Table 5.4 below presents a comparison between the average ricochet debris particle diameters and velocities presented in Reference [2] and the average particle velocities and diameters calculated using equations (5.1a,b) and (5.2a,b) under the same impact conditions. As can be seen from this table, the average diameter values predicted by the equations developed in this study compare favorably with those obtained previously. However, the average velocity values calculated using equations (5.1a,b) and (5.2a,b) are approximately twice the values reported previously. These differences and similarities serve to 1) reinforce the need to explore further the particle velocities obtained using the technique developed in this study, and 2) increase the confidence in the particle diameter values obtained using this technique.

Table 5.4 Comparison of Average Ricochet Particle Diameters and Velocities

	d_{avg} (cm)		V_{avg} (km/s)	
θ_p (deg)	Reference [2]	This Study	Reference [2]	This Study
45	0.174	0.121	2.07	4.25
60	0.221	0.204	2.01	4.42
75	0.357	0.348	2.35	4.78
	d_{avg} (cm)		V_{avg} (km/s)	
d_p (cm)	Reference [2]	This Study	Reference [2]	This Study
0.475	0.203	0.164	2.17	4.35
0.635	0.258	0.224	2.15	4.49
0.795	0.303	0.285	2.08	4.61

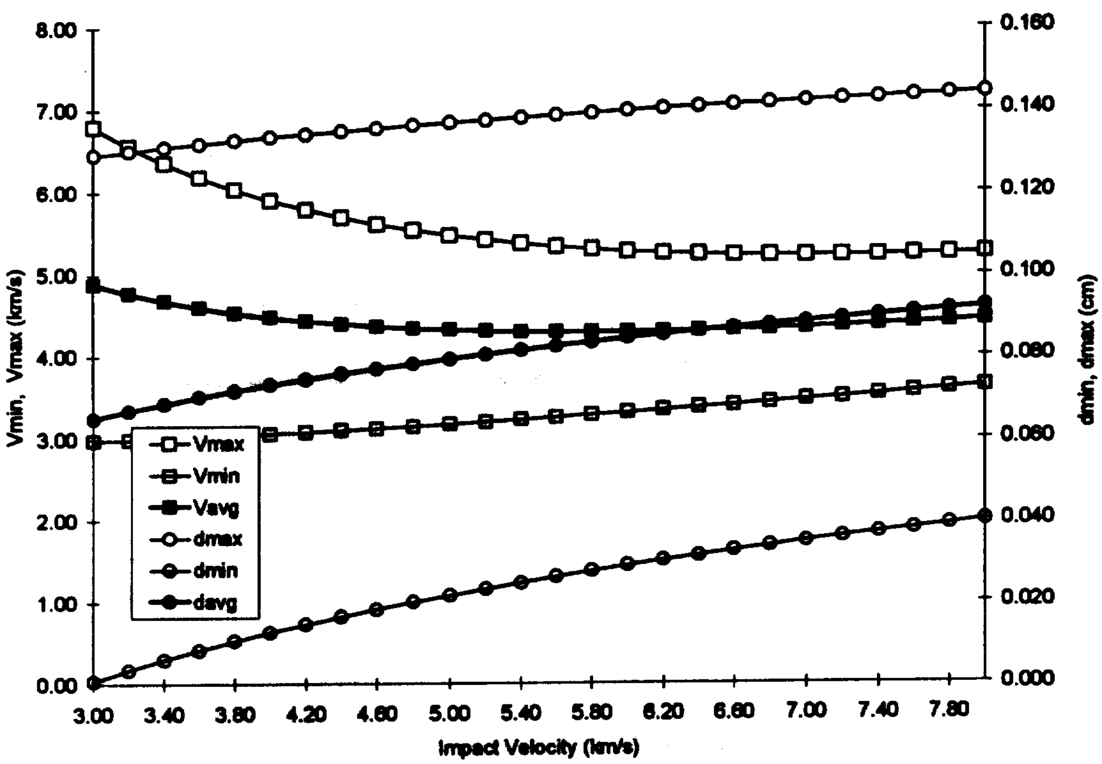

Figure 5.3 V_{min}, V_{max} and d_{min}, d_{max} for a 30° Impact

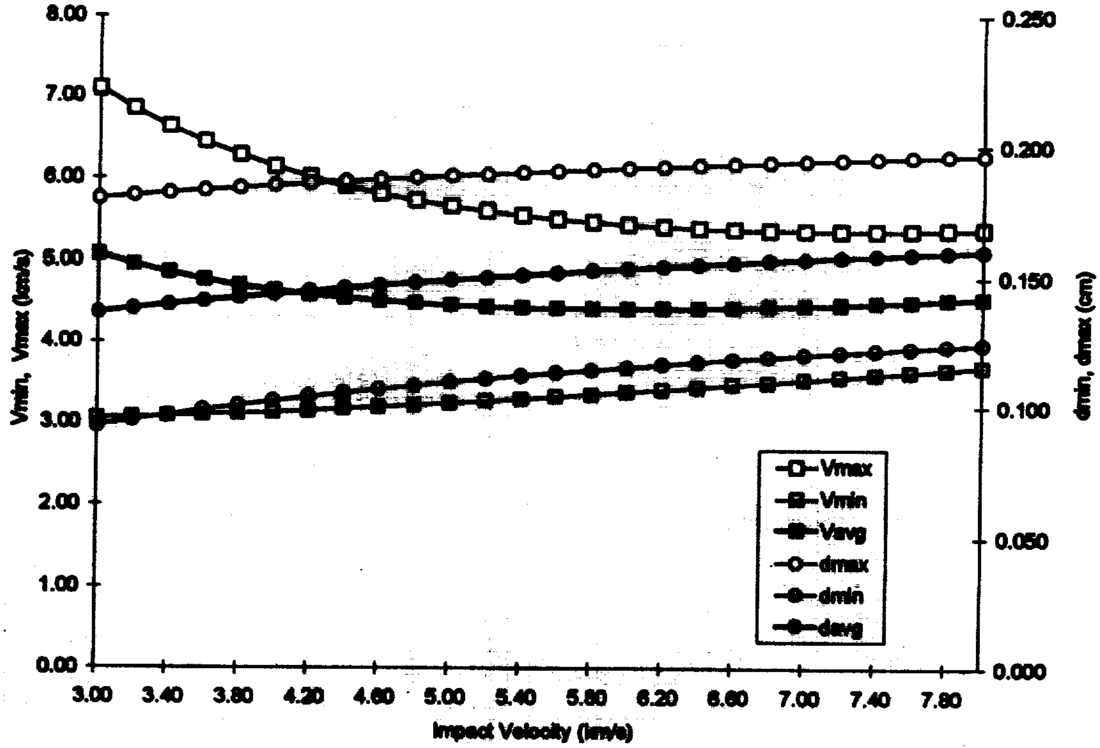

Figure 5.4 V_{min}, V_{max} and d_{min}, d_{max} for a 45° Impact

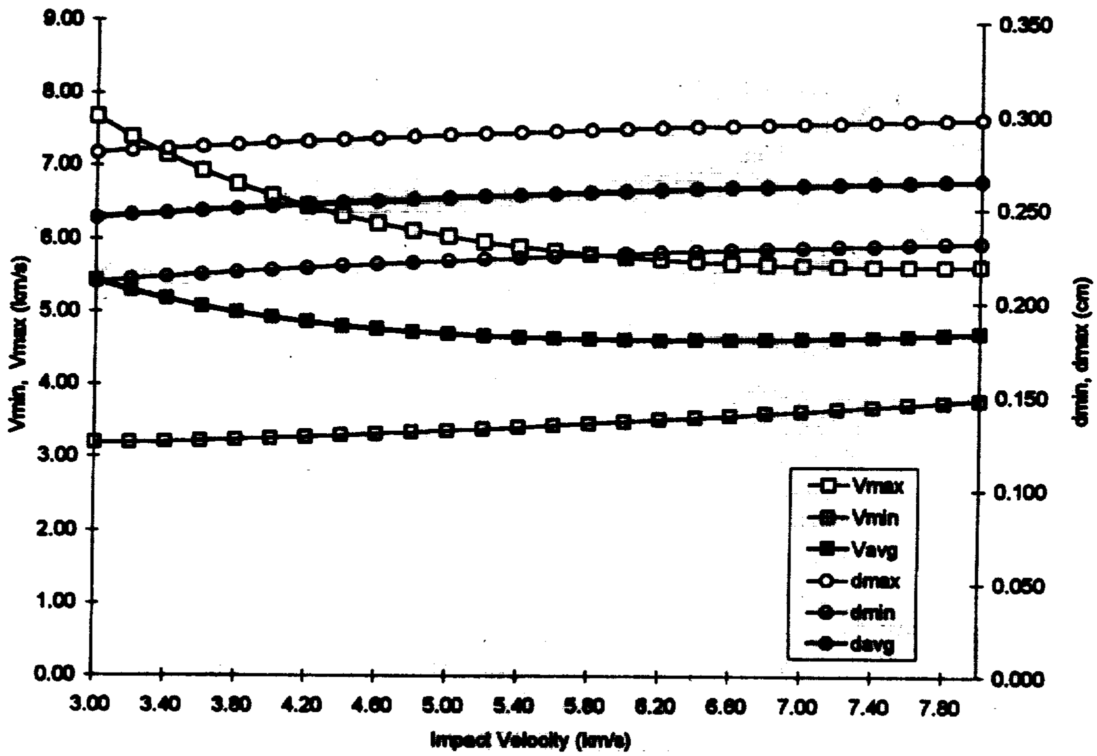

Figure 5.5 V_{min}, V_{max} and d_{min}, d_{max} for a 60° Impact

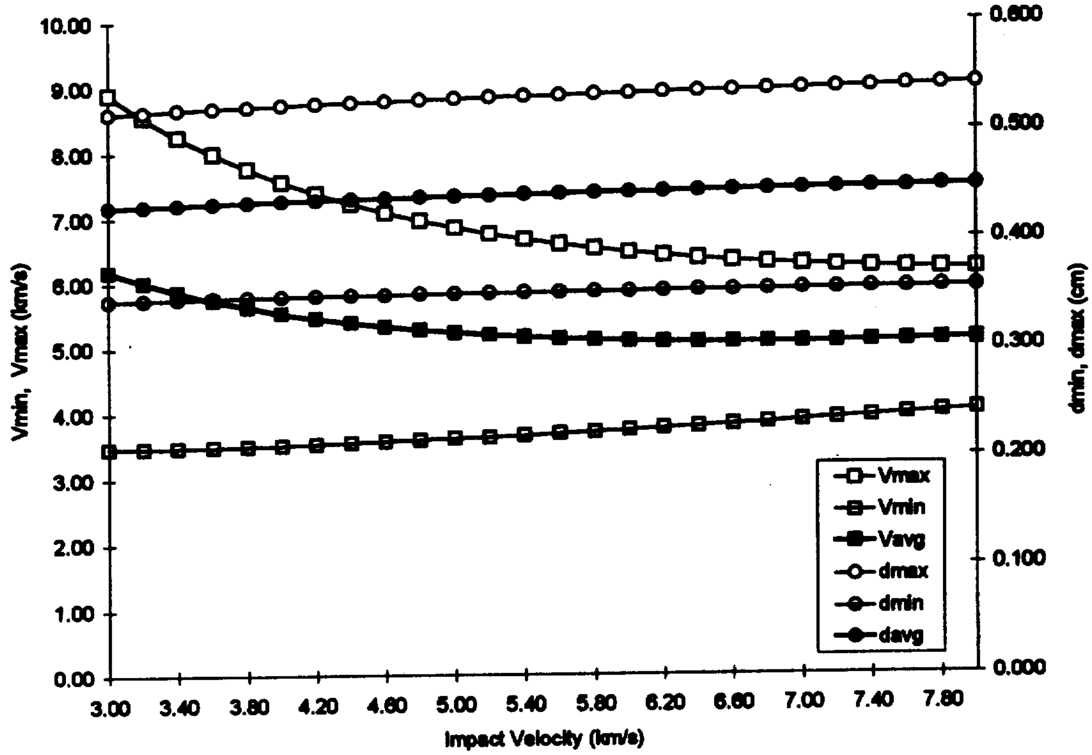

Figure 5.6 V_{min}, V_{max} and d_{min}, d_{max} for a 75° Impact

6.0 SUMMARY AND RECOMMENDATIONS

6.1 Summary

An empirical model that that characterizes the secondary ejecta created by a high speed impact on a typical aerospace structural surface has been successfully developed. This model developed provides the following information as a function of impact parameters (speed, angle, projectile diameter) and target plate geometry (e.g. thickness, etc):

- angles defining the spread of ricochet debris and the trajectory of the ricochet debris cloud center-of-mass;
- average velocity of the ricochet debris cloud material; and,
- velocity and mass of the largest particle(s) in the ricochet debris cloud.

The angles defining the spread of the ricochet debris cloud and the trajectory of the debris cloud center-of-mass were obtained using the spatial distributions of ricochet debris particle impacts on ricochet witness plates from over 200 high speed impact tests. The average velocity of the ricochet debris cloud is obtained using a model that characterizes the masses, trajectories, and velocities of the debris clouds created in an oblique high-speed impact. This model employs the three conservation principles, elementary shock physics theory, and fundamental thermodynamic principles to obtain a system of algebraic equations for the various debris cloud masses, trajectories, and velocities. Finally, relationships for crater diameter and depth are applied to the deepest craters in each ricochet witness plate to "back out" the diameters, masses, and velocities of the ricochet debris cloud particles that created these craters. This information is then used to develop empirical relationships that predict the velocity and mass of the largest ricochet debris cloud particle in terms of impact parameters and bumper plate thickness.

6.2 Recommendations

Based on the work performed, the following recommendations are made for continued activities in this area.

6.2.1 Ricochet Debris Cloud Spread Angle Modelling

1) The discrepancy between empirical observations and SPH predictions of ricochet debris cloud spread should be explored and reconciled. It is suggested that an alternative means of defining ricochet debris cloud spread needs to be developed, one that will allow the successful use of empirical as well as numerical data.
2) Thus far, ricochet debris cloud spread angle modelling efforts have focussed on characterizing the spread of the debris cloud particles "in the plane of the impact trajectory". Future efforts should focus on the spread of the debris cloud out of this plane.

6.2.2 Ricochet Debris Cloud Velocity Modelling

Efforts should continue to reduce the dependence of the model on empirical or user-controlled parameters. A preliminary effort involving oblique shock wave theory was successfully completed by the author [8]; however, the modelling effort was at a level of complexity that is inconsistent with that employed in the model presented in this report. Some aspects of oblique shock wave theory should, however, be explored and considered for implementation in the debris cloud model presented herein.

6.2.3 Ricochet Debris Cloud Particle Diameter and Velocity Modelling

The reasons for the differences between the values of the correlation coefficients for the empirical diameter and velocity equations should be explored and reconciled, including the consideration of an alternative equation form should be considered for the ricochet debris cloud particle velocity.

7.0 REFERENCES

1. W.P. Schonberg and F. Yang, "Response of Spacecraft Structures to Orbital Debris Particle Impact," *International Journal of Impact Engineering*, Vol. 14, 1993, pp. 647-658.

2. W.P. Schonberg and R.A. Taylor, "Exterior Spacecraft Subsystem Protective Shielding Analysis and Design," *Journal of Spacecraft and Rockets*, Vol. 27, 1990, pp. 267-274.

3. G. T. Burch, Multi-plate Damage Study, AFATL-TR-67-116, Eglin Air Force Base, Florida, 1967.

4. W.P. Schonberg and R.A Taylor, "Penetration and Ricochet Phenomena in Oblique Hypervelocity Impact," *AIAA Journal*, Vol. 27, No. 5, 1989, pp. 639-646.

5. W. P. Schonberg, A. J. Bean and K. Darzi, Hypervelocity Impact Physics, NASA CR-4343, Washington, D.C., 1991.

6. M.H. Rice, R.G. McQueen, and J.M. Walsh, "Compression of Solids by Strong Shock Waves," Solid State Physics, Volume VI, (ed. F. Seitz and D. Turnbull), Academic Press, New York, 1958.

7. C.A. Anderson, T.G. Trucano, and S.A. Mullin, "Debris Cloud Dynamics," *International Journal of Impact Engineering*, Vol. 9, No. 1, 1990, pp. 89-113.

8. Schonberg, W.P. and Ebrahim, A.R., "Modelling Oblique Hypervelocity Impact Phenomena Using Elementary Shock Physics," *International Journal of Impact Engineering*, to appear, 1999.

9. Sawle, D.R., "Hypervelocity Impact in Thin Sheets and Semi-Infinite Targets at 15 km/sec," *AIAA Journal*, Vol.8, No.7, 1970, pp. 1240-1244.

10. Bruce, E.P., "Review and Analysis of High Velocity Impact Data," Proceedings of the Fifth Hypervelocity Impact Symposium, 1962, pp. 439-474.

11. Schneider, E., "Velocity Dependence of Some Impact Phenomena," Proceedings of the Comet Halley Micrometeoroid Hazard Workshop, ESA SP-1 53, ESA Scientific and Technical Publications Branch, The Netherlands, 1979, pp. 101 - 107.

12. Goodman, E.H., and Liles, C.D., "Particle-Solid Impact Phenomena," Proceedings of the Sixth Hypervelocity Impact Symposium, 1963, pp. 543-577

13. Dunn, W P., "On Material Strengths of the Hypervelocity Impact Problem," *AJAA Journal*, Vol.4, No.3, 1966, pp. 535-536.

14. Sedgwick, R.T., Hageman, L.J., Herrmann, R.G., and Waddell, J.L., "Numerical Investigations in Penetration Mechanics," *International Journal of Engineering Sciences*, Vol.16, 1978, pp. 859-869.

15. Christman, D.R., "Target Strength and Hypervelocity Impact," *AIAA Journal*, Vol.4, No. 10, 1966, pp. 1872-1874.

16. Summers, J.L., and Charters, A.C., "High-Speed Impact of Metal Projectiles in Targets of Various Materials" Proceedings of the Third Hypervelocity Impact Symposium, 1959, pp. 101-113.

17. Sorenson, N.R., "Systematic Investigation of Crater Formation in Metals," Proceedings of the Seventh Hypervelocity Impact Symposium, 1962, Vol. 6, pp. 281-325.

18. Herrmann, W., and Jones, A.H., "Correlation of Hypervelocity Impact Data," Proceedings of the Fifth Hypervelocity Impact Symposium, 1962, pp. 389-438.

19. Cour-Palais, B.G., "Hypervelocity Impact Investigations and Meteoroid Shielding Experience Related to Apollo and Skylab," Orbital Debris, NASA CP-2360, 1982, pp. 247-275.

20. Summers, J.L., Investigation of High Speed Impact: Regions of impact and Impact at Oblique Angles, NASA TN D-94, 1959.

APPENDIX A

EMPIRICAL TEST PARAMETERS AND RESULTS

Table A-1 Empirical Test Parameters and Results, Phase B NASA/MSFC Test Series

Test No.	t_b (cm)	d_p (cm)	V_p (cm)	θ_p (cm)	θ_r (cm)	θ_{99} (cm)
001A	0.203	0.795	6.62	45	11.3	26.3
001B	0.203	0.795	6.53	45	12.6	26.9
002A	0.160	0.795	6.50	45	9.5	23.0
002B	0.160	0.795	6.45	45	12.1	26.0
003A	0.102	0.795	6.54	45	6.0	20.9
004A	0.203	0.795	6.28	65	7.6	25.3
136A	0.160	0.635	6.25	55	8.6	25.1
136B	0.160	0.635	7.24	55	10.8	29.2
136C	0.160	0.635	6.67	55	13.0	28.8
137D	0.081	0.635	7.03	45	9.6	24.7
150A	0.160	0.635	7.00	45	11.4	24.2
151A	0.203	0.635	6.88	45	13.5	21.5
154A	0.102	0.475	6.83	45	11.1	19.2
155A	0.160	0.475	7.02	45	12.6	18.1
156A	0.160	0.475	7.10	65	6.8	16.9
156B	0.160	0.475	5.95	65	7.7	19.2
156C	0.160	0.475	4.15	65	7.1	16.5
157A	0.160	0.475	7.40	60	10.0	22.3
162A	0.160	0.475	6.53	30	16.7	31.0
168A	0.081	0.635	5.54	45	8.8	19.3
168B	0.081	0.635	5.98	45	10.8	25.1
168C	0.081	0.635	6.67	45	19.4	29.9
168D	0.081	0.635	7.02	45	21.7	30.8
169B	0.081	0.635	6.55	45	10.8	25.1
201A	0.102	0.635	4.33	45	10.4	23.3
201B	0.102	0.635	5.51	45	8.8	23.1
201D	0.102	0.635	7.59	45	14.3	22.8
202C	0.102	0.475	5.25	45	10.8	23.3
202D	0.102	0.475	6.44	45	6.2	14.6
202E	0.102	0.475	7.19	45	6.3	16.0
203A	0.102	0.762	4.79	65	7.0	21.6
203B	0.102	0.762	3.65	65	7.2	19.8
203C	0.102	0.762	2.72	65	6.8	21.0
203D	0.102	0.762	5.59	65	6.4	22.2
203E	0.102	0.762	6.72	65	8.1	23.5
203F	0.102	0.889	3.05	65	8.5	26.0
203G	0.102	0.889	4.64	65	8.1	25.5
204A	0.102	0.635	4.77	65	8.5	24.2
204B	0.102	0.635	5.86	65	7.9	24.0
204C	0.102	0.635	4.25	65	9.0	28.2

204D	0.102	0.635	3.18	65	5.3	18.4
205A	0.160	0.635	4.16	45	7.9	22.6
205B	0.160	0.635	4.61	45	7.5	22.8
205C	0.160	0.635	5.30	45	11.6	22.6
205D	0.160	0.635	6.30	45	13.3	24.5
205E	0.160	0.635	3.15	45	9.9	22.2
206E	0.160	0.475	3.24	45	10.9	21.9
206F	0.160	0.475	6.15	45	9.1	26.6
207A	0.160	0.762	5.74	65	6.8	20.5
207B	0.160	0.762	6.25	65	6.2	23.4
207C	0.160	0.762	7.03	65	6.7	20.9
208C	0.160	0.635	3.32	65	7.8	19.5
208D	0.160	0.635	5.63	65	5.8	13.1
208E	0.160	0.635	6.47	65	7.0	22.8
209A	0.160	0.635	4.29	65	5.8	21.4
209B	0.160	0.635	6.35	65	6.5	24.4
209D	0.160	0.635	7.34	65	12.0	32.0
210B	0.160	0.889	5.69	65	7.9	23.5
210D	0.160	0.889	6.93	65	12.0	25.7
211B	0.160	0.889	5.87	45	12.6	29.4
211D	0.160	0.889	6.97	45	13.9	28.7
212B	0.160	0.762	6.27	45	15.4	28.7
216A	0.203	0.889	5.99	45	13.2	25.2
216B	0.203	0.889	6.54	45	12.9	25.2
216C	0.203	0.795	6.91	45	11.0	26.0
217A	0.102	0.795	6.59	45	4.6	9.1
217B	0.102	0.795	7.10	45	4.6	9.1
217C	0.102	0.635	6.05	45	5.5	13.5
217D	0.102	0.635	6.47	45	6.2	16.4
217E	0.102	0.635	7.14	45	8.4	16.3
218A	0.102	0.889	5.82	45	10.2	29.2
218B	0.102	0.889	6.30	45	10.6	23.3
218C	0.102	0.889	6.82	45	7.6	23.7
221A	0.102	0.475	6.42	45	3.5	8.0
221B	0.102	0.475	5.93	45	9.7	24.2
221C	0.102	0.475	4.60	45	11.4	28.7
221D	0.102	0.475	4.08	45	10.9	22.3
222A	0.102	0.318	5.60	45	7.6	19.7
222B	0.102	0.318	5.03	45	12.8	25.7
222C	0.102	0.318	3.33	45	11.0	23.5
226A	0.081	0.635	4.45	45	6.6	16.4
226B	0.081	0.635	5.49	45	10.0	23.5
226C	0.081	0.635	6.73	45	15.0	23.3
227A	0.081	0.635	5.58	45	8.3	26.0

227B	0.081	0.635	7.19	45	13.8	25.6
230A	0.160	0.475	4.41	45	18.8	23.9
230B	0.160	0.475	3.23	45	10.8	21.8
230C	0.160	0.635	5.18	45	11.2	26.6
230D	0.160	0.635	5.55	45	10.4	27.0
230E	0.160	0.635	6.57	45	12.7	24.9
231A	0.160	0.475	3.34	65	5.4	19.4
231B	0.160	0.475	2.44	65	5.9	27.2
231C	0.160	0.795	6.59	65	8.1	20.9
231D	0.160	0.795	7.26	65	9.4	23.3
301-	0.160	0.635	2.94	45	9.0	19.3
303-	0.160	0.795	4.65	45	9.6	21.0
303A	0.160	0.795	3.72	45	8.2	17.5
303B	0.160	0.795	4.42	45	8.5	18.3
306-	0.160	0.953	6.35	45	10.1	18.4
319-	0.102	0.795	2.99	45	8.4	20.0
320-	0.160	0.795	3.08	45	9.8	22.6
321-	0.203	0.795	3.01	45	8.4	23.3
324-	0.102	0.795	4.12	45	9.3	24.0
325-	0.160	0.795	4.25	45	8.7	23.3
326-	0.203	0.795	4.25	45	11.0	25.2
333-	0.102	0.475	2.93	45	9.6	25.5
334-	0.102	0.475	3.66	45	10.6	24.0
335-	0.102	0.635	4.12	45	9.4	23.1
336-	0.102	0.635	4.54	45	9.9	20.9
336A	0.102	0.635	5.76	45	12.5	24.2
337-	0.102	0.795	6.90	45	12.2	25.0
338-	0.102	0.795	7.02	45	12.4	25.2
339-	0.102	0.953	6.55	45	8.5	26.9

Table A-2 Empirical Test Parameters and Results, Phase C/D NASA/MSFC Test Series

Test No.	t_b (cm)	d_p (cm)	V_p (cm)	θ_p (cm)	θ_r (cm)	θ_{99} (cm)
4001-A	0.203	0.795	3.15	45	13.6	33.7
4001-B	0.203	0.795	4.29	45	12.3	28.4
4001-C	0.203	0.795	6.12	45	12.1	33.7
4001-D	0.203	0.795	6.71	45	16.5	33.0
4002-A	0.203	0.795	3.20	75	7.4	22.1
4002-B	0.203	0.795	3.97	75	7.9	26.6
4002-C	0.203	0.795	6.30	75	6.2	21.8
4002-D	0.160	0.795	7.14	75	7.0	20.9
4002-E	0.203	0.795	6.41	75	4.3	16.7
4003-A	0.160	0.795	3.43	45	11.2	32.3
4003-B	0.203	0.795	6.29	45	14.6	34.9
4003-C	0.203	0.795	3.18	45	13.3	29.5
4003-D	0.203	0.795	6.22	45	12.1	31.5
4004-A	0.203	0.795	3.19	75	5.6	18.6
4004-B	0.203	0.795	6.08	75	8.3	26.0
4004-C	0.203	0.795	6.19	75	5.6	20.6
4100-A	0.127	0.475	3.00	45	11.1	25.3
4100-B	0.127	0.475	3.78	45	12.4	29.9
4100-C	0.127	0.475	5.66	45	7.6	23.3
4100-D	0.127	0.475	7.20	45	17.3	28.4
4101-A	0.127	0.635	3.14	45	9.5	27.0
4101-B	0.127	0.635	4.13	45	11.6	30.4
4101-C	0.127	0.635	6.14	45	9.0	28.4
4101-D	0.127	0.635	7.52	45	12.8	28.4
4102-A	0.127	0.795	2.95	45	8.3	18.6
4102-B	0.127	0.795	4.12	45	5.2	14.3
4102-C	0.127	0.795	6.24	45	6.7	19.2
4102-C1	0.127	0.795	6.05	45	11.3	29.5
4102-C2	0.127	0.795	6.02	45	6.3	19.0
4102-D	0.127	0.795	7.18	45	6.4	19.3
4103-A	0.127	0.475	2.94	60	10.4	25.8
4103-B	0.127	0.475	3.98	60	7.9	25.1
4103-C	0.127	0.475	5.88	60	20.0	37.4
4103-D	0.127	0.475	7.37	60	5.5	13.7
4104-A	0.127	0.635	7.23	60	9.5	29.1
4104-B	0.127	0.635	4.19	60	8.1	27.6
4104-C	0.127	0.635	6.12	60	8.0	28.9
4104-D	0.127	0.635	7.52	60	15.9	29.5
4105-A	0.127	0.795	2.92	60	4.9	21.0
4105-A1	0.127	0.795	2.98	60	7.6	23.5

4105-B	0.127	0.795	4.02	60	7.3	25.1
4105-C	0.127	0.795	6.15	60	7.6	24.8
4105-D	0.127	0.795	7.23	60	7.6	25.5
4106-A	0.127	0.475	3.05	60	9.4	26.8
4106-A1	0.127	0.475	3.10	75	4.8	16.3
4106-B	0.127	0.475	4.12	60	12.7	28.7
4106-B1	0.127	0.475	3.99	75	4.1	16.1
4106-C	0.127	0.475	5.95	75	4.3	19.0
4106-D	0.127	0.475	7.56	75	5.8	22.4
4107-A	0.127	0.635	3.05	75	6.5	22.8
4107-B	0.127	0.635	4.11	75	5.8	24.9
4107-C	0.127	0.635	6.20	75	6.0	20.6
4107-D	0.127	0.635	7.64	75	6.1	23.0
4108-A	0.127	0.795	3.12	75	7.0	22.6
4108-A1	0.127	0.795	2.95	75	5.4	18.7
4108-B	0.127	0.795	3.97	75	6.7	22.8
4108-C	0.127	0.795	5.96	75	6.9	23.5
4108-D	0.127	0.795	7.07	75	6.5	22.6
4109-A	0.203	0.475	3.27	45	14.7	39.4
4109-B	0.203	0.475	4.14	45	15.3	31.8
4109-C	0.203	0.475	6.53	45	13.2	29.5
4109-D	0.203	0.475	7.46	45	25.6	34.8
4110-A	0.203	0.635	3.25	45	16.1	32.3
4110-B	0.203	0.635	4.00	45	22.3	32.3
4110-C	0.203	0.635	5.76	45	18.4	30.6
4110-D	0.203	0.635	6.96	45	17.5	33.6
4111-A	0.203	0.795	2.85	45	19.3	33.0
4111-B	0.203	0.795	3.94	45	17.6	35.0
4111-C	0.203	0.795	5.97	45	20.9	35.5
4111-D	0.203	0.795	6.81	45	18.4	36.9
4112-A	0.203	0.475	3.33	60	10.2	29.1
4112-B	0.203	0.475	4.05	60	8.9	26.8
4112-C	0.203	0.475	5.87	60	12.8	31.0
4112-D	0.203	0.475	7.50	60	14.4	28.0
4113-A	0.203	0.635	2.97	60	7.1	29.8
4113-B	0.203	0.635	3.77	60	12.1	41.0
4113-C	0.203	0.635	6.30	60	10.1	28.0
4113-D	0.203	0.635	7.12	60	10.2	31.0
4114-A	0.203	0.795	3.13	60	9.5	27.8
4114-B	0.203	0.795	3.98	60	12.4	32.0
4114-C	0.203	0.795	5.92	60	13.3	28.9
4114-D	0.203	0.795	7.40	60	10.0	31.8
4115-A	0.203	0.475	3.13	75	7.0	19.5
4115-B	0.203	0.475	4.08	75	6.1	13.1

4115-C	0.203	0.475	6.06	75	9.3	30.0
4115-D	0.203	0.475	7.30	75	6.0	24.7
4116-A	0.203	0.635	2.92	75	4.4	17.5
4116-B	0.203	0.635	4.48	75	8.7	27.4
4116-C	0.203	0.635	6.24	75	5.8	20.3
4116-D	0.203	0.635	7.36	75	7.3	22.8
4117-A	0.203	0.795	3.11	75	5.3	18.0
4117-B	0.203	0.795	4.05	75	7.7	22.6
4117-C	0.203	0.795	6.03	75	6.5	26.9
4117-D	0.203	0.795	7.20	75	6.8	25.5

Table A-3 Empirical Test Parameters and Results, NASA/MSFC EH Test Series

Test No.	t_b (cm)	d_p (cm)	V_p (cm)	θ_p (cm)	θ_r (cm)	θ_{99} (cm)
EH1AA	0.160	0.795	6.93	75	9.5	31.1
EH1AB	0.160	0.795	6.91	75	7.4	27.2
EH1AP	0.160	0.795	6.82	75	9.3	29.8
EH1B	0.160	0.795	7.01	45	15.5	29.3
EH1BP	0.160	0.635	7.22	75	6.6	27.5
EH1C	0.160	0.795	7.17	60	10.6	27.9
EH1CP	0.160	0.475	7.52	75	8.2	25.1
EH1D	0.160	0.795	7.16	75	7.9	29.0
EHRP1	0.160	0.795	6.93	60	10.6	24.2
EHRP2	0.160	0.795	6.85	65	8.7	21.2
EHRP3	0.160	0.795	6.83	45	12.5	27.7
EHRP4	0.160	0.635	7.71	60	10.8	26.0
EHRP5	0.160	0.635	7.56	65	13.0	30.1
EHRP6	0.160	0.635	7.63	45	11.5	24.5
EHRP7	0.160	0.475	8.04	60	18.5	30.8
EHRP8	0.160	0.475	7.39	45	11.9	27.2
EHRP9	0.160	0.475	7.34	65	13.8	34.1
EHSS4C	0.160	0.635	5.58	45	9.9	28.9

APPENDIX B

SPH NUMERICAL SIMULATION PARAMETERS AND RESULTS

Table B-1 SPH Numerical Simulation Parameters and Results

Test No.	t_b (cm)	d_p (cm)	V_p (km/s)	θ_p (deg)	θ_r (deg)	θ_{99} (deg)
SPH-01	0.160	0.635	7	45	24	40
SPH-02	0.160	0.635	7	60	13	28
SPH-03	0.160	0.635	7	75	4	11
SPH-04	0.160	0.635	11	45	21	39
SPH-05	0.160	0.635	11	60	12	29
SPH-06	0.160	0.635	11	75	5	10
SPH-07	0.160	0.635	15	45	17	33
SPH-08	0.160	0.635	15	60	12	23
SPH-09	0.160	0.635	15	75	4	11
SPH-10	0.160	0.953	7	45	16	40
SPH-11	0.160	0.953	7	60	12	26
SPH-12	0.160	0.953	7	75	5	12
SPH-13	0.160	0.953	11	45	28	40
SPH-14	0.160	0.953	11	60	12	21
SPH-15	0.160	0.953	11	75	4	11
SPH-16	0.160	0.953	15	45	20	40
SPH-17	0.160	0.953	15	60	10	22
SPH-18	0.160	0.953	15	75	5	13
SPH-19	0.160	1.270	7	45	25	41
SPH-20	0.160	1.270	7	60	14	25
SPH-21	0.160	1.270	7	75	6	14
SPH-22	0.160	1.270	11	45	23	40
SPH-23	0.160	1.270	11	60	10	24
SPH-24	0.160	1.270	11	75	5	14
SPH-25	0.160	1.270	15	45	19	39
SPH-26	0.160	1.270	15	60	11	20
SPH-27	0.160	1.270	15	75	4	10
SPH-28	0.127	0.795	9	45	18	40
SPH-29	0.127	0.795	9	60	11	20
SPH-30	0.127	0.795	9	75	5	12
SPH-31	0.127	0.795	13	45	24	41
SPH-32	0.127	0.795	13	60	13	23
SPH-33	0.127	0.795	13	75	8	14
SPH-34	0.127	1.113	9	45	20	41
SPH-35	0.127	1.113	9	60	13	23
SPH-36	0.127	1.113	9	75	5	14
SPH-37	0.127	1.113	13	45	24	41
SPH-38	0.127	1.113	13	60	13	25
SPH-39	0.127	1.113	13	75	6	14

APPENDIX C

MEASURED CRATER DEPTHS AND DIAMETERS

Table C-1 Measured Crater Depths and Diameters, Calculated Crater Volumes
Phase B NASA/MSFC Test Series

Test No.	V_p (km/s)	θ_p (deg)	d_p (cm)	t_b (cm)	p_1 (cm)	d_1 (cm)	Vol_1 ($x10^{-2}$ cm^3)	p_2 (cm)	d_2 (cm)	Vol_2 ($x10^{-2}$ cm^3)	p_3 (cm)	d_3 (cm)	Vol_3 ($x10^{-2}$ cm^3)
001B	6.56	45	0.795	0.20	0.042	0.095	0.020	0.043	0.088	0.017	0.046	0.101	0.025
002B	6.51	45	0.795	0.16	0.033	0.113	0.022	0.040	0.095	0.019	0.041	0.088	0.017
201A	4.33	45	0.635	0.10	0.026	0.055	0.004	0.028	0.071	0.007	0.026	0.056	0.004
205A	4.20	45	0.635	0.16	0.037	0.084	0.014	0.018	0.099	0.009	0.048	0.088	0.015
205C	5.30	45	0.635	0.16	0.018	0.071	0.005	0.033	0.071	0.009	0.024	0.082	0.008
205D	6.42	45	0.635	0.16	0.018	0.074	0.005	0.029	0.092	0.013	0.024	0.062	0.005
205E	3.15	45	0.635	0.16	0.023	0.089	0.010						
206E	3.24	45	0.462	0.16	0.012	0.070	0.003	0.014	0.048	0.002			
206F	6.42	45	0.475	0.16	0.037	0.061	0.005	0.006	0.052	0.001			
211B	5.88	45	0.889	0.16	0.058	0.105	0.025	0.035	0.089	0.015	0.047	0.101	0.025
211D	6.84	45	0.889	0.16	0.052	0.105	0.030	0.024	0.111	0.015	0.035	0.091	0.015
212B	6.38	45	0.762	0.16	0.031	0.096	0.015	0.026	0.081	0.009	0.019	0.091	0.008
216A	6.10	45	0.889	0.20	0.058	0.101	0.023	0.038	0.112	0.025	0.039	0.067	0.007
216C	6.96	45	0.795	0.20	0.045	0.119	0.033	0.058	0.131	0.052	0.045	0.103	0.025
217A	6.65	45	0.795	0.10	0.036	0.098	0.018	0.028	0.099	0.014	0.029	0.099	0.015
217B	7.10	45	0.795	0.10	0.077	0.092	0.026	0.032	0.076	0.010	0.031	0.076	0.009
217C	6.05	45	0.635	0.10	0.036	0.076	0.011	0.029	0.068	0.007			
217D	6.47	45	0.635	0.10	0.029	0.088	0.012	0.026	0.072	0.007			
217E	7.14	45	0.635	0.10	0.018	0.071	0.005	0.031	0.058	0.004			
218A	5.82	45	0.889	0.10	0.040	0.115	0.028	0.036	0.087	0.014	0.042	0.096	0.020
218C	6.88	45	0.889	0.10	0.063	0.121	0.036	0.032	0.098	0.016	0.031	0.072	0.008
221B	5.97	45	0.475	0.10	0.020	0.076	0.006	0.029	0.058	0.004			
221C	4.62	45	0.475	0.10	0.012	0.032	0.001						
226A	4.48	45	0.635	0.08	0.004	0.062	0.001						
226B	5.49	45	0.635	0.08	0.015	0.052	0.002	0.027	0.098	0.014			
227A	5.64	45	0.635	0.08	0.102	0.085	0.029	0.030	0.085	0.011	0.020	0.085	0.008
227B	7.25	45	0.635	0.08	0.027	0.082	0.010						
230B	3.23	45	0.475	0.16	0.036	0.085	0.014	0.038	0.086	0.015			
230C	5.16	45	0.635	0.16	0.024	0.081	0.008	0.030	0.090	0.013	0.021	0.088	0.009
230D	5.51	45	0.635	0.16	0.023	0.086	0.009	0.045	0.088	0.014	0.028	0.063	0.006
230E	6.62	45	0.635	0.16	0.043	0.112	0.028	0.021	0.065	0.005			
301-	2.95	45	0.635	0.16	0.026	0.086	0.010	0.027	0.084	0.010	0.012	0.076	0.004
303-	4.59	45	0.795	0.16	0.062	0.082	0.016	0.046	0.081	0.012	0.078	0.101	0.031
303A	3.65	45	0.795	0.16	0.016	0.131	0.014	0.031	0.088	0.013	0.022	0.081	0.008
303B	4.34	45	0.795	0.16	0.040	0.086	0.015	0.033	0.085	0.012	0.075	0.074	0.016
319-	2.93	45	0.795	0.10	0.042	0.061	0.006	0.029	0.084	0.011			
321-	2.97	45	0.795	0.20	0.071	0.091	0.023	0.043	0.098	0.022	0.026	0.069	0.006
324-	4.05	45	0.795	0.10	0.016	0.101	0.009	0.025	0.088	0.010	0.018	0.085	0.007
325-	4.14	45	0.795	0.16	0.026	0.088	0.011	0.029	0.084	0.011	0.036	0.073	0.010
326-	4.22	45	0.795	0.20	0.105	0.151	0.094	0.076	0.138	0.057	0.060	0.131	0.054
333-	2.88	45	0.475	0.10	0.020	0.068	0.005						

334-	3.61	45	0.475	0.10	0.012	0.031	0.001						
335-	4.07	45	0.635	0.10	0.012	0.066	0.003	0.019	0.067	0.004			
336-	4.47	45	0.635	0.10	0.033	0.061	0.005	0.023	0.069	0.006			
336A	5.70	45	0.635	0.10	0.027	0.091	0.012	0.022	0.076	0.007	0.023	0.059	0.004
337-	6.81	45	0.795	0.10	0.026	0.081	0.009	0.033	0.087	0.013	0.020	0.091	0.009
338-	6.98	45	0.795	0.10	0.034	0.078	0.011	0.026	0.106	0.015	0.016	0.069	0.004

Table C-2 Measured Crater Depths and Diameters, Calculated Crater Volumes
Phase C/D NASA/MSFC Test Series

Test No.	V_p (km/s)	θ_p (deg)	d_p (cm)	t_b (cm)	p_1 (cm)	d_1 (cm)	Vol_1 ($x10^{-2}$ cm^3)	p_2 (cm)	d_2 (cm)	Vol_2 ($x10^{-2}$ cm^3)	p_3 (cm)	d_3 (cm)	Vol_3 ($x10^{-2}$ cm^3)
4001A	3.15	45	0.795	0.20	0.021	0.085	0.008	0.018	0.086	0.007	0.039	0.109	0.024
4001B	4.29	45	0.795	0.20	0.053	0.103	0.022	0.033	0.089	0.014	0.036	0.096	0.017
4001C	6.12	45	0.795	0.20	0.045	0.138	0.045	0.073	0.119	0.041	0.038	0.101	0.020
4001D	6.71	45	0.795	0.20	0.029	0.104	0.016	0.040	0.104	0.023	0.035	0.084	0.013
4002B	3.97	75	0.795	0.20	0.194	0.282	0.606	0.174	0.184	0.231	0.214	0.161	0.218
4002D	7.14	75	0.795	0.16	0.500	0.226	1.003	0.319	0.161	0.325	0.308	0.132	0.211
4002E	6.41	75	0.795	0.20	0.500	0.204	0.817	0.314	0.137	0.231	0.381	0.187	0.523
4003A	3.43	45	0.795	0.16	0.041	0.086	0.016	0.040	0.082	0.014	0.024	0.081	0.008
4003B	6.29	45	0.795	0.20	0.052	0.065	0.009	0.035	0.091	0.015	0.029	0.065	0.006
4003C	3.18	45	0.795	0.20	0.019	0.091	0.008	0.032	0.088	0.013	0.039	0.071	0.008
4003D	6.22	45	0.795	0.20	0.058	0.079	0.014	0.029	0.095	0.014	0.033	0.101	0.018
4004A	3.19	75	0.795	0.20	0.211	0.202	0.338	0.124	0.251	0.409	0.155	0.232	0.328
4004B	6.08	75	0.795	0.20	0.291	0.151	0.261	0.261	0.201	0.414	0.230	0.191	0.329
4101A	3.14	45	0.635	0.13	0.029	0.065	0.006						
4101B	4.13	45	0.635	0.13	0.029	0.085	0.011	0.035	0.076	0.011	0.135	0.074	0.029
4101C	6.14	45	0.635	0.13	0.041	0.124	0.033	0.015	0.105	0.009			
4102A	2.95	45	0.795	0.13	0.031	0.084	0.011	0.041	0.088	0.017	0.041	0.081	0.011
4102C	6.24	45	0.795	0.13	0.042	0.088	0.017	0.046	0.110	0.029	0.062	0.081	0.016
4102C1	6.05	45	0.795	0.13	0.035	0.131	0.031	0.062	0.065	0.010	0.032	0.081	0.011
4103A	2.94	60	0.475	0.13	0.006	0.042	0.001						
4103B	3.98	60	0.475	0.13	0.067	0.134	0.047	0.042	0.119	0.031	0.042	0.104	0.024
4103C	5.88	60	0.475	0.13	0.041	0.086	0.016	0.026	0.109	0.016	0.043	0.078	0.010
4103D	7.37	60	0.475	0.13	0.053	0.118	0.039	0.040	0.135	0.038	0.038	0.088	0.015
4104A	7.23	60	0.635	0.13	0.051	0.115	0.035	0.083	0.116	0.044	0.058	0.074	0.012
4104B	4.19	60	0.635	0.13	0.049	0.136	0.047	0.068	0.084	0.019	0.037	0.081	0.013
4104C	6.12	60	0.635	0.13	0.079	0.114	0.040	0.067	0.152	0.081	0.051	0.136	0.049
4104D	7.52	60	0.635	0.13	0.051	0.124	0.041	0.037	0.101	0.020	0.054	0.095	0.019
4105A	2.92	60	0.795	0.13	0.071	0.111	0.034	0.065	0.165	0.093	0.115	0.204	0.188
4105A1	2.98	60	0.795	0.13	0.057	0.117	0.041	0.062	0.118	0.034	0.090	0.126	0.056
4105B	4.02	60	0.795	0.13	0.139	0.117	0.075	0.070	0.174	0.111	0.053	0.148	0.061
4106A	3.05	60	0.475	0.13	0.052	0.102	0.021	0.039	0.101	0.021	0.039	0.116	0.027
4106A1	3.10	75	0.475	0.13	0.128	0.131	0.086	0.118	0.112	0.058	0.127	0.185	0.171
4106B	4.12	60	0.475	0.13	0.044	0.105	0.025	0.025	0.118	0.018	0.058	0.091	0.019
4106B1	3.99	75	0.475	0.13	0.118	0.181	0.152	0.128	0.191	0.183	0.091	0.131	0.061
4106C	5.95	75	0.475	0.13	0.129	0.186	0.175	0.091	0.221	0.233	0.058	0.196	0.117
4106D	7.56	75	0.475	0.13	0.160	0.241	0.365	0.241	0.149	0.210	0.066	0.159	0.087
4107A	3.05	75	0.475	0.13	0.106	0.214	0.254	0.121	0.274	0.476	0.104	0.085	0.030
4107B	4.11	75	0.635	0.13	0.161	0.263	0.437	0.132	0.221	0.253	0.124	0.194	0.183
4107C	6.20	75	0.635	0.13	0.238	0.174	0.283	0.185	0.221	0.355	0.191	0.115	0.099
4107D	7.64	75	0.635	0.13	0.254	0.164	0.268	0.301	0.175	0.362	0.218	0.139	0.165
4108A	3.12	75	0.795	0.13	0.214	0.406	1.385	0.266	0.229	0.548	0.139	0.204	0.227

4108A1	2.95	75	0.838	0.13	0.321	0.212	0.567	0.171	0.144	0.139	0.151	0.186	0.205
4108B	3.97	75	0.795	0.13	0.251	0.269	0.713	0.151	0.225	0.300	0.135	0.121	0.078
4109A	3.27	45	0.475	0.20	0.010	0.055	0.002						
4109B	4.14	45	0.475	0.20	0.017	0.074	0.005	0.027	0.057	0.005			
4109C	6.53	45	0.475	0.20	0.021	0.075	0.006	0.011	0.069	0.003			
4110A	3.25	45	0.635	0.20	0.045	0.076	0.010	0.050	0.064	0.008	0.027	0.075	0.008
4110B	4.00	45	0.635	0.20	0.014	0.074	0.004	0.032	0.071	0.008			
4110C	5.76	45	0.635	0.20	0.014	0.059	0.003	0.013	0.079	0.004	0.018	0.092	0.008
4110D	6.96	45	0.635	0.20	0.029	0.114	0.020	0.030	0.119	0.022	0.054	0.066	0.009
4111A	2.85	45	0.795	0.20	0.017	0.078	0.005	0.024	0.122	0.019			
4111B	3.94	45	0.795	0.20	0.063	0.134	0.059	0.049	0.079	0.012	0.039	0.081	0.013
4111C	5.97	45	0.795	0.20	0.045	0.079	0.011	0.046	0.073	0.010	0.051	0.123	0.040
4111D	6.81	45	0.795	0.20	0.052	0.101	0.021	0.060	0.075	0.013	0.024	0.091	0.010
4112A	3.33	60	0.475	0.20	[illegible]	[illegible]	0.022	0.048	0.110	0.030	0.027	0.116	0.019
4112B	4.05	60	0.475	0.20	0.091	0.121	0.052	0.061	0.055	0.007	0.032	0.119	0.024
4112C	5.87	60	0.475	0.20	0.030	0.114	0.020	0.054	0.092	0.018	0.059	0.086	0.017
4112D	7.50	60	0.475	0.20	0.043	0.085	0.012	0.064	0.101	0.026	0.059	0.135	0.056
4113A	2.97	60	0.635	0.20	0.070	0.152	0.085	0.055	0.069	0.010	0.065	0.069	0.012
4113B	3.77	60	0.635	0.20	0.077	0.135	0.055	0.070	0.102	0.029	0.032	0.087	0.013
4113C	6.30	60	0.635	0.20	0.161	0.175	0.194	0.072	0.141	0.056	0.099	0.112	0.049
4113D	7.12	60	0.635	0.20	0.051	0.161	0.069	0.125	0.095	0.044	0.102	0.079	0.025
4114A	3.13	60	0.795	0.20	0.114	0.115	0.059	0.094	0.134	0.066	0.093	0.169	0.104
4114B	3.98	60	0.795	0.20	0.136	0.091	0.044	0.101	0.093	0.034	0.085	0.081	0.022
4114C	5.92	60	0.795	0.20	0.131	0.156	0.125	0.112	0.101	0.045	0.105	0.115	0.055
4114D	7.40	60	0.795	0.20	0.095	0.186	0.129	0.091	0.176	0.111	0.101	0.078	0.024
4115A	3.13	75	0.475	0.20	0.139	0.192	0.201	0.084	0.092	0.028	0.049	0.092	0.016
4115B	4.08	75	0.475	0.20	0.084	0.100	0.033	0.112	0.169	0.126	0.063	0.129	0.055
4115C	6.06	75	0.475	0.20	0.195	0.145	0.161	0.139	0.091	0.045	0.139	0.085	0.039
4115D	7.30	75	0.475	0.20	0.168	0.189	0.236	0.181	0.174	0.215	0.139	0.138	0.104
4116A	2.92	75	0.635	0.20	0.171	0.146	0.143	0.161	0.175	0.194	0.052	0.118	0.038
4116B	4.84	75	0.635	0.20	0.108	0.158	0.106	0.123	0.212	0.217	0.068	0.181	0.117
4116C	6.24	75	0.635	0.20	0.151	0.292	0.506	0.174	0.191	0.249	0.166	0.192	0.240
4116D	7.36	75	0.635	0.20	0.321	0.154	0.299	0.271	0.222	0.524	0.139	0.101	0.056
4117A	3.11	75	0.795	0.20	0.178	0.201	0.282	0.169	0.134	0.119	0.139	0.125	0.085
4117B	4.05	75	0.795	0.20	0.500	0.159	0.496	0.180	0.131	0.121	0.179	0.129	0.117
4117C	6.03	75	0.795	0.20	0.489	0.181	0.629	0.534	0.182	0.695	0.327	0.177	0.402
4117D	7.20	75	0.795	0.20	0.477	0.176	0.580	0.384	0.139	0.291	0.231	0.141	0.180

Table C-3 Measured Crater Depths and Diameters, Calculated Crater Volumes
NASA/MSFC EH Test Series

Test No.	V_p (km/s)	θ_p (deg)	d_p (cm)	t_b (cm)	p_1 (cm)	d_1 (cm)	Vol_1 ($x10^{-2}$ cm^3)	p_2 (cm)	d_2 (cm)	Vol_2 ($x10^{-2}$ cm^3)	p_3 (cm)	d_3 (cm)	Vol_3 ($x10^{-2}$ cm^3)
EHAB	6.91	75	0.795	0.16	0.615	0.734	13.011	0.368	0.686	6.801	0.483	0.566	6.076
EHPB	7.22	75	0.635	0.16	0.495	0.650	8.213	0.361	0.602	5.138	0.310	0.445	2.411
EHPC	7.58	75	0.475	0.16	0.386	0.599	5.439	0.318	0.447	2.495	0.345	0.422	2.413
EHRP1	6.87	60	0.795	0.16	0.140	0.254	0.355	0.094	0.241	0.286	0.117	0.244	0.365
EHRP2	6.80	65	0.795	0.16	0.371	0.632	5.819	0.229	0.445	1.781	0.211	0.445	2.188
EHRP3	6.78	45	0.795	0.16	0.165	0.368	1.170	0.150	0.320	0.804	0.135	0.343	0.832
EHRP4	7.65	60	0.635	0.16	0.152	0.279	0.465	0.216	0.371	1.168	0.157	0.328	0.884
EHRP5	7.51	65	0.635	0.16	0.305	0.528	3.339	0.330	0.546	3.863	0.203	0.411	1.795
EHRP6	7.57	45	0.635	0.16	0.097	0.201	0.205	0.114	0.267	0.426	0.084	0.211	0.196
EHRP7	7.98	60	0.475	0.16	0.323	0.488	3.021	0.254	0.396	1.564	0.203	0.465	2.298
EHRP8	7.34	45	0.475	0.16	0.155	0.262	0.418	0.137	0.279	0.558	0.168	0.295	0.574
EHRP9	7.29	65	0.475	0.16	0.108	0.221	0.276	0.096	0.266	0.356	0.089	0.197	0.181
EHSS4C	5.53	45	0.635	0.16	0.078	0.126	0.049	0.074	0.139	0.056	0.045	0.088	0.014

APPENDIX D

EMPIRICAL DEPTH AND DIAMETERS EQUATIONS

Penetration Depth Equations

$p/d = 2.28(\rho_p/\rho_b)^{2/3}(V_p/C_b)^{2/3}$	[9]	(D.1)
$p/d = 1.96(\rho_p/\rho_b)^{1/2}(V_p/C_b)^{2/3}$	[10]	(D.2)
$p/d_p = 1.50(\rho_p/\rho_b)^{1/3}(\rho_p V_p^2/2S_b)^{1/3}$	[11]	(D.3)
$p/\ d_p = 2.35(\rho_p/\rho_b)^{0.70}(V_p/C_b)^{2/3}$	[12]	(D.4)
$p/d_p = 0.63(\rho_p V_p^2/S_{yt})^{1/3}$	[13]	(D.5)
$p/d_p = 0.428(\rho_p/\rho_b)^{0.537}(V_p/C_b)^{0.576}(Y_b/\rho_b C_b^2)^{-0.235}$	[14]	(D.6)
$p/d_p = 8.355\text{x}10^{-4}\rho p2/3\rho b\text{-}1/3(V_p^2/H_b)^{1/3}$	[15]	(D.7)
$p/d_p = 2.00(\rho_p/\rho_b)^{4.52}(V_p/C_b)^{1/136}$	[16]	(D.8)
$p/d_p = 0.311(\rho_p/\rho_b)^{0.17}(\rho_p V_p^2/S_b)^{1/3}$	[17]	(D.9)
$p/d_p = 0.36(\rho_p/\rho_b)^{2/3}(\rho_p V_p^2/B_b)^{1/3}$	[18]	(D.10)
$p = 2.973\text{x}10^{-7}d_p^{1.1}H_b^{-0.25}\rho_p^{0.5}\rho_b^{-0.167}V_p^{4/3}$	[19]	(D.11)
$p = 1.129\text{x}10^{-6}d_p^{1.056}H_b^{-0.25}\rho_p^{0.5}\rho_b^{-0.167}E_t^{-0.33}V_p^{4/3}$	[19]	(D.12)

Crater Mouth Diameter Equations

$\alpha d^2p/d_p^3 = 34(\rho_p/\rho_b)^{3/2}(V_p/C_b)^2$	[20]	(D.13)
$\alpha d^2p/d_p^3 = 0.120(\rho_p/\rho_b)^{1/2}(\rho_p V_p^2/S_b)^{0.845}$	[17]	(D.14)
$\alpha d^2p/d_p^3 = 30.25(\rho_p/\rho_b)^{3/2}(V_p/C_b)^2$	[10]	(D.15)
$\alpha d^2p/d_p^3 = 44.10(\rho_p/\rho_b)^{3/2}(V_p/C_b)^2$	[12]	(D.16)
$\alpha d^2p/d_p^3 = 2.65\text{x}10^{-9}\rho_p^{7/6}\rho_b^{-1/2}V_p^{4/3}/\ H_b$	[15]	(D.17)
$\alpha d^2p/d_p^3 = 0.16(\rho_p/\rho_b)^{2/3}\rho_p V_p^2/B_b$	[18]	(D.18)

where α=0.75 if $p>d/2$ and α=1.00 if $p<d/2$.

APPENDIX E

CALCULATED RICOCHET PARTICLE VELOCITIES AND DIAMETERS

Test No.	p	d	V7-14	D7-14	D7-14/d	V10-14	D10-14	D10-14/d	V2-14	D2-14	D2-14/d
No.	(cm)	(cm)									
EHAB	0.615	0.734	[illegible]	[illegible]	[illegible]	[illegible]	[illegible]	[illegible]	[illegible]	[illegible]	[illegible]
EHPB	0.495	0.650	[illegible]	[illegible]	[illegible]	[illegible]	[illegible]	[illegible]	[illegible]	[illegible]	[illegible]
EHPC	0.386	0.599	[illegible]	[illegible]	[illegible]	[illegible]	[illegible]	[illegible]	3.828	0.237	0.395
EHRP1	0.117	0.244	3.949	0.094	0.387	7.520	0.066	0.269	[illegible]	[illegible]	[illegible]
EHRP2	0.371	0.632	[illegible]	[illegible]	[illegible]	[illegible]	[illegible]	[illegible]	2.097	0.340	0.537
EHRP3	0.165	0.368	2.560	0.178	0.483	4.876	0.124	0.336	[illegible]	[illegible]	[illegible]
EHRP4	0.216	0.371	[illegible]	[illegible]	[illegible]	[illegible]	[illegible]	[illegible]	1.989	0.205	0.552
EHRP5	0.330	0.546	[illegible]	[illegible]	[illegible]	[illegible]	[illegible]	[illegible]	2.531	0.266	0.488
EHRP6	0.114	0.267	1.868	0.152	0.568	3.556	0.105	0.395	[illegible]	[illegible]	[illegible]
EHRP7	0.323	0.488	[illegible]	[illegible]	[illegible]	[illegible]	[illegible]	[illegible]	4.549	0.176	0.362
EHRP8	0.137	0.279	4.603	0.100	0.358	8.766	0.069	0.249	[illegible]	[illegible]	[illegible]
EHRP9	0.244	0.676	[illegible]	[illegible]	[illegible]	1.202	0.465	0.688	[illegible]	[illegible]	[illegible]
EHSS4C	0.188	0.353	[illegible]	[illegible]	[illegible]	[illegible]	[illegible]	[illegible]	1.116	0.262	0.742
001B	0.117	0.257	2.833	0.118	0.459	5.394	0.082	0.319	[illegible]	[illegible]	[illegible]
002B	0.084	0.287	[illegible]	[illegible]	[illegible]	[illegible]	[illegible]	[illegible]	[illegible]	[illegible]	[illegible]
201A	0.071	0.180	1.119	0.133	0.738	2.130	0.093	0.513	[illegible]	[illegible]	[illegible]
205A	0.122	0.224	[illegible]	[illegible]	[illegible]	[illegible]	[illegible]	[illegible]	1.306	0.153	0.685
205C	0.084	0.180	3.229	0.077	0.429	6.149	0.054	0.298	[illegible]	[illegible]	[illegible]
205D	0.074	0.234	[illegible]	[illegible]	[illegible]	[illegible]	[illegible]	[illegible]	[illegible]	[illegible]	[illegible]
205E	0.058	0.226	[illegible]	[illegible]	[illegible]	[illegible]	[illegible]	[illegible]	[illegible]	[illegible]	[illegible]
206E	0.030	0.178	[illegible]	[illegible]	[illegible]	[illegible]	[illegible]	[illegible]	[illegible]	[illegible]	[illegible]
206F	0.094	0.155	[illegible]	[illegible]	[illegible]	[illegible]	[illegible]	[illegible]	2.590	0.075	0.482
211B	0.147	0.267	[illegible]	[illegible]	[illegible]	[illegible]	[illegible]	[illegible]	1.416	0.175	0.657
211D	0.132	0.267	4.863	0.093	0.348	9.261	0.065	0.242	[illegible]	[illegible]	[illegible]
212B	0.079	0.244	[illegible]	[illegible]	[illegible]	[illegible]	[illegible]	[illegible]	[illegible]	[illegible]	[illegible]
216A	0.097	0.284	[illegible]	[illegible]	[illegible]	0.807	0.240	0.844	[illegible]	[illegible]	[illegible]
216C	0.147	0.333	2.360	0.168	0.504	4.495	0.117	0.350	[illegible]	[illegible]	[illegible]
217A	0.091	0.249	0.708	0.232	0.933	1.348	0.162	0.649	[illegible]	[illegible]	[illegible]
217B	0.196	0.234	[illegible]	[illegible]	[illegible]	[illegible]	[illegible]	[illegible]	[illegible]	[illegible]	[illegible]
217C	0.091	0.193	3.649	0.078	0.403	6.950	0.054	0.280	[illegible]	[illegible]	[illegible]
217D	0.074	0.224	[illegible]	[illegible]	[illegible]	[illegible]	[illegible]	[illegible]	[illegible]	[illegible]	[illegible]
217E	0.046	0.180	[illegible]	[illegible]	[illegible]	[illegible]	[illegible]	[illegible]	[illegible]	[illegible]	[illegible]
218A	0.102	0.292	[illegible]	[illegible]	[illegible]	0.947	0.227	0.777	[illegible]	[illegible]	[illegible]
218C	0.160	0.307	[illegible]	[illegible]	[illegible]	[illegible]	[illegible]	[illegible]	0.967	0.245	0.799
221B	0.051	0.193	[illegible]	[illegible]	[illegible]	[illegible]	[illegible]	[illegible]	[illegible]	[illegible]	[illegible]
221C	0.030	0.081	0.808	0.071	0.871	1.539	0.049	0.606	[illegible]	[illegible]	[illegible]
226A	0.010	0.157	[illegible]	[illegible]	[illegible]	[illegible]	[illegible]	[illegible]	[illegible]	[illegible]	[illegible]
226B	0.069	0.249	[illegible]	[illegible]	[illegible]	[illegible]	[illegible]	[illegible]	[illegible]	[illegible]	[illegible]
227A	0.259	0.216	[illegible]	[illegible]	[illegible]	[illegible]	[illegible]	[illegible]	[illegible]	[illegible]	[illegible]
227B	0.069	0.208	[illegible]	[illegible]	[illegible]	0.665	0.194	0.931	[illegible]	[illegible]	[illegible]
230B	0.097	0.218	2.330	0.111	0.507	4.437	0.077	0.353	[illegible]	[illegible]	[illegible]
230C	0.076	0.229	[illegible]	[illegible]	[illegible]	0.720	0.204	0.894	[illegible]	[illegible]	[illegible]
230D	0.114	0.224	[illegible]	[illegible]	[illegible]	[illegible]	[illegible]	[illegible]	0.861	0.189	0.847
230E	0.109	0.284	0.941	0.229	0.806	1.792	0.160	0.561	[illegible]	[illegible]	[illegible]
301-	0.066	0.218	[illegible]	[illegible]	[illegible]	[illegible]	[illegible]	[illegible]	[illegible]	[illegible]	[illegible]
303-	0.198	0.257	[illegible]	[illegible]	[illegible]	[illegible]	[illegible]	[illegible]	[illegible]	[illegible]	[illegible]
303A	0.041	0.333	[illegible]	[illegible]	[illegible]	[illegible]	[illegible]	[illegible]	[illegible]	[illegible]	[illegible]
303B	0.191	0.188	[illegible]	[illegible]	[illegible]	[illegible]	[illegible]	[illegible]	[illegible]	[illegible]	[illegible]
319-	0.074	0.213	[illegible]	[illegible]	[illegible]	0.903	0.170	0.797	[illegible]	[illegible]	[illegible]
321-	0.180	0.231	[illegible]	[illegible]	[illegible]	[illegible]	[illegible]	[illegible]	[illegible]	[illegible]	[illegible]
324-	0.064	0.224	[illegible]	[illegible]	[illegible]	[illegible]	[illegible]	[illegible]	[illegible]	[illegible]	[illegible]
325-	0.066	0.224	[illegible]	[illegible]	[illegible]	[illegible]	[illegible]	[illegible]	[illegible]	[illegible]	[illegible]
326-	0.267	0.384	[illegible]	[illegible]	[illegible]	[illegible]	[illegible]	[illegible]	6.255	0.118	0.307
333-	0.051	0.173	[illegible]	[illegible]	[illegible]	[illegible]	[illegible]	[illegible]	[illegible]	[illegible]	[illegible]
334-	0.030	0.079	[illegible]	[illegible]	[illegible]	1.889	0.043	0.546	[illegible]	[illegible]	[illegible]
335-	0.048	0.170	[illegible]	[illegible]	[illegible]	[illegible]	[illegible]	[illegible]	[illegible]	[illegible]	[illegible]

336-	0.058	0.175									
336A	0.069	0.231									
337-	0.064	0.221				1.657	0.120	[illegible]			
338-	0.066	[illegible]									
4001A	0.090	0.277				1.137	[illegible]	[illegible]			
4001B	0.136	0.262									
4001C	0.114	0.351									
4001D	0.102	0.284	[illegible]	0.212	[illegible]	[illegible]	0.147	[illegible]			
4002B	0.493	0.716							5.836	0.228	0.318
4002D	1.270	0.674									
4002E	1.270	0.518									
4003A	0.104	0.218	3.804	0.086	[illegible]	7.244	0.080	0.274			
4003B	0.089	0.231	[illegible]	0.185	[illegible]	1.613	0.129	[illegible]			
4003C	0.081	0.224				1.202	0.150	[illegible]			
4003D	0.084	0.257									
4004A	0.315	0.638	4.787	0.224	0.351	9.116	0.158	0.244			
4004B	0.663	0.511									
4101A	0.074	0.165	2.450	0.081	0.491	4.723	0.058	0.342			
4101B	0.343	0.188									
4101C	0.104	0.316									
4102A	0.104	0.224	3.280	0.085	[illegible]	6.246	0.058	[illegible]			
4102C	0.117	0.279	1.633	0.170	[illegible]	3.110	0.118	[illegible]			
4102C1	0.069	0.333									
4103A	0.015	0.107									
4103B	0.170	0.340									
4103C	0.104	0.218	3.804	0.086	[illegible]	7.244	0.080	0.274			
4103D	0.135	0.300	2.589	0.144	[illegible]	4.931	0.100	0.384			
4104A	0.211	0.295							7.521	0.082	0.280
4104B	0.124	0.345				1.189	0.239	0.692			
4104C	0.170	0.386	2.294	0.197	0.511	4.368	0.137	0.358			
4104D	0.130	0.315	1.487	0.202	0.642	2.794	0.141	0.447			
4105A	0.292	0.518							1.615	0.318	0.614
4105A1	0.229	0.320							7.437	0.090	0.281
4105B	0.178	0.442	1.272	0.305	0.691	2.422	0.212	0.481			
4106A	0.099	0.295				0.761	0.256	0.869			
4106A1	0.325	0.333									
4106B	0.112	0.267	1.655	0.161	0.604	3.152	0.112	0.420			
4106B1	0.325	0.485							4.929	0.168	0.347
4106C	0.231	0.561	1.478	0.359	0.640	2.815	0.250	0.445			
4106D	0.406	0.612							4.639	0.219	0.358
4107A	0.307	0.698	[illegible]	0.354	[illegible]	[illegible]	0.240	[illegible]			
4107B	0.409	0.668							2.749	0.313	0.468
4107C	0.470	0.561									
4107D	0.765	0.445									
4108A	0.544	1.031							1.047	0.791	0.767
4108A1	0.815	0.538									
4108B	0.638	0.683									
4109A	0.025	0.140									
4109B	0.043	0.188									
4109C	0.053	0.191									
4110A	0.114	0.193							2.217	0.101	[illegible]
4110B	0.081	0.180	2.648	0.086	[illegible]	5.042	0.059	[illegible]			
4110C	0.046	0.234									
4110D	0.076	0.302									
4111A	0.061	0.310									
4111B	0.160	0.340	3.477	0.141	0.413	6.622	0.098	0.287			
4111C	0.130	0.312	1.546	0.195	0.625	2.944	0.136	0.435			
4111D	0.132	0.257	[illegible]	[illegible]	[illegible]	[illegible]	[illegible]	[illegible]	0.900	0.213	0.829

4112A	0.122	0.279	2.149	0.148	0.528	4.093	0.103	0.368	[redacted]			
4112B	0.231	0.307	[redacted]									
4112C	0.076	0.290	[redacted]									
4112D	0.150	0.343	2.171	0.180	0.526	4.134	0.125	0.366	[redacted]			
4113A	0.178	0.386	3.043	0.171	0.442	5.795	0.119	0.308	[redacted]			
4113B	0.196	0.343	[redacted]						1.742	0.203	0.591	
4113C	0.409	0.445	[redacted]									
4113D	0.130	0.409	[redacted]									
4114A	0.236	0.429	[redacted]						1.382	0.286	0.665	
4114B	0.345	0.231	[redacted]									
4114C	0.333	0.396	[redacted]									
4114D	0.241	0.472	[redacted]									
4115A	0.353	0.488	[redacted]						8.112	0.131	0.269	
4115B	0.160	0.328	4.444	0.119	0.364	8.463	0.083	0.253	[redacted]			
4115C	0.495	0.368	[redacted]									
4115D	0.427	0.480	[redacted]									
4116A	0.409	0.445	[redacted]									
4116B	0.312	0.538	[redacted]						1.944	0.301	0.559	
4116C	0.384	0.742	[redacted]									
4116D	0.688	0.564	[redacted]									
4117A	0.452	0.511	[redacted]									
4117B	1.270	0.404	[redacted]									
4117C	1.356	0.462	[redacted]									
4117D	1.212	0.447	[redacted]									

Test No.	p	d	V5-14	D5-14	D5-14/d	V1-14	D1-14	D1-14/d	V4-14	D4-14	D4-14/d
No.	(cm)	(cm)									
EHAB	0.615	0.734	[illegible]	[illegible]	[illegible]	4.819	0.278	0.379	3.596	0.328	0.447
EHPB	0.495	0.650	5.628	0.218	0.336	2.002	0.337	0.519	1.642	0.398	0.612
EHPC	0.386	0.599	1.016	0.349	0.583	[illegible]	[illegible]	[illegible]	[illegible]	[illegible]	[illegible]
EHRP1	0.117	0.244	[illegible]	[illegible]	[illegible]	[illegible]	[illegible]	[illegible]	[illegible]	[illegible]	[illegible]
EHRP2	0.371	0.632	1.050	0.502	0.794	[illegible]	[illegible]	[illegible]	[illegible]	[illegible]	[illegible]
EHRP3	0.165	0.366	[illegible]	[illegible]	[illegible]	[illegible]	[illegible]	[illegible]	[illegible]	[illegible]	[illegible]
EHRP4	0.216	0.371	0.995	0.303	0.816	[illegible]	[illegible]	[illegible]	[illegible]	[illegible]	[illegible]
EHRP5	0.330	0.546	1.207	0.394	0.721	[illegible]	[illegible]	[illegible]	[illegible]	[illegible]	[illegible]
EHRP6	0.114	0.267	[illegible]	[illegible]	[illegible]	[illegible]	[illegible]	[illegible]	[illegible]	[illegible]	[illegible]
EHRP7	0.323	0.485	[illegible]	0.261	[illegible]	[illegible]	0.402	0.825	0.780	0.475	0.972
EHRP8	0.157	0.278	[illegible]	[illegible]	[illegible]	[illegible]	[illegible]	[illegible]	[illegible]	[illegible]	[illegible]
EHRP9	0.244	0.676	[illegible]	[illegible]	[illegible]	[illegible]	[illegible]	[illegible]	[illegible]	[illegible]	[illegible]
[illegible]	0.188	0.383	[illegible]	[illegible]	[illegible]	[illegible]	[illegible]	[illegible]	[illegible]	[illegible]	[illegible]
001B	0.117	0.257	[illegible]	[illegible]	[illegible]	[illegible]	[illegible]	[illegible]	[illegible]	[illegible]	[illegible]
002B	[illegible]	[illegible]	[illegible]	[illegible]	[illegible]	[illegible]	[illegible]	[illegible]	[illegible]	[illegible]	[illegible]
201A	0.071	0.180	[illegible]	[illegible]	[illegible]	[illegible]	[illegible]	[illegible]	[illegible]	[illegible]	[illegible]
206A	0.122	0.224	[illegible]	[illegible]	[illegible]	[illegible]	[illegible]	[illegible]	[illegible]	[illegible]	[illegible]
206C	0.094	0.180	[illegible]	[illegible]	[illegible]	[illegible]	[illegible]	[illegible]	[illegible]	[illegible]	[illegible]
206D	0.074	0.224	[illegible]	[illegible]	[illegible]	[illegible]	[illegible]	[illegible]	[illegible]	[illegible]	[illegible]
[illegible]	0.056	0.226	[illegible]	[illegible]	[illegible]	[illegible]	[illegible]	[illegible]	[illegible]	[illegible]	[illegible]
206E	0.030	0.178	[illegible]	[illegible]	[illegible]	[illegible]	[illegible]	[illegible]	[illegible]	[illegible]	[illegible]
206F	0.094	0.155	[illegible]	0.110	[illegible]	[illegible]	[illegible]	[illegible]	[illegible]	[illegible]	[illegible]
211B	0.147	0.267	[illegible]	[illegible]	[illegible]	[illegible]	[illegible]	[illegible]	[illegible]	[illegible]	[illegible]
211D	0.132	0.267	[illegible]	[illegible]	[illegible]	[illegible]	[illegible]	[illegible]	[illegible]	[illegible]	[illegible]
212B	0.079	0.244	[illegible]	[illegible]	[illegible]	[illegible]	[illegible]	[illegible]	[illegible]	[illegible]	[illegible]
216A	0.097	0.284	[illegible]	[illegible]	[illegible]	[illegible]	[illegible]	[illegible]	[illegible]	[illegible]	[illegible]
216C	0.147	0.333	[illegible]	[illegible]	[illegible]	[illegible]	[illegible]	[illegible]	[illegible]	[illegible]	[illegible]
217A	0.091	0.249	[illegible]	[illegible]	[illegible]	[illegible]	[illegible]	[illegible]	[illegible]	[illegible]	[illegible]
217B	0.196	0.234	[illegible]	[illegible]	[illegible]	4.785	0.089	0.380	3.571	0.105	0.448
217C	0.091	0.193	[illegible]	[illegible]	[illegible]	[illegible]	[illegible]	[illegible]	[illegible]	[illegible]	[illegible]
217D	0.074	0.224	[illegible]	[illegible]	[illegible]	[illegible]	[illegible]	[illegible]	[illegible]	[illegible]	[illegible]
217E	0.046	0.180	[illegible]	[illegible]	[illegible]	[illegible]	[illegible]	[illegible]	[illegible]	[illegible]	[illegible]
218A	0.102	0.292	[illegible]	[illegible]	[illegible]	[illegible]	[illegible]	[illegible]	[illegible]	[illegible]	[illegible]
218C	0.160	0.307	[illegible]	[illegible]	[illegible]	[illegible]	[illegible]	[illegible]	[illegible]	[illegible]	[illegible]
221B	0.051	0.193	[illegible]	[illegible]	[illegible]	[illegible]	[illegible]	[illegible]	[illegible]	[illegible]	[illegible]
221C	0.030	0.081	[illegible]	[illegible]	[illegible]	[illegible]	[illegible]	[illegible]	[illegible]	[illegible]	[illegible]
226A	0.010	0.157	[illegible]	[illegible]	[illegible]	[illegible]	[illegible]	[illegible]	[illegible]	[illegible]	[illegible]
226B	0.069	0.249	[illegible]	[illegible]	[illegible]	[illegible]	[illegible]	[illegible]	[illegible]	[illegible]	[illegible]
227A	0.259	0.216	[illegible]	[illegible]	[illegible]	[illegible]	[illegible]	[illegible]	[illegible]	[illegible]	[illegible]
227B	0.069	0.208	[illegible]	[illegible]	[illegible]	[illegible]	[illegible]	[illegible]	[illegible]	[illegible]	[illegible]
230B	0.097	0.218	[illegible]	[illegible]	[illegible]	[illegible]	[illegible]	[illegible]	[illegible]	[illegible]	[illegible]
230C	0.076	0.229	[illegible]	[illegible]	[illegible]	[illegible]	[illegible]	[illegible]	[illegible]	[illegible]	[illegible]
230D	0.114	0.224	[illegible]	[illegible]	[illegible]	[illegible]	[illegible]	[illegible]	[illegible]	[illegible]	[illegible]
230E	0.109	0.284	[illegible]	[illegible]	[illegible]	[illegible]	[illegible]	[illegible]	[illegible]	[illegible]	[illegible]
301-	0.066	0.218	[illegible]	[illegible]	[illegible]	[illegible]	[illegible]	[illegible]	[illegible]	[illegible]	[illegible]
303-	0.198	0.257	6.160	0.082	0.321	2.848	0.127	0.496	2.125	0.150	0.584
303A	0.041	0.333	[illegible]	[illegible]	[illegible]	[illegible]	[illegible]	[illegible]	[illegible]	[illegible]	[illegible]
303B	0.191	0.188	[illegible]	[illegible]	[illegible]	[illegible]	[illegible]	[illegible]	[illegible]	[illegible]	[illegible]
319-	0.074	0.213	[illegible]	[illegible]	[illegible]	[illegible]	[illegible]	[illegible]	[illegible]	[illegible]	[illegible]
321-	0.180	0.231	6.580	0.072	0.310	3.042	0.111	0.479	2.270	0.131	0.565
324-	0.064	0.224	[illegible]	[illegible]	[illegible]	[illegible]	[illegible]	[illegible]	[illegible]	[illegible]	[illegible]
325-	0.066	0.224	[illegible]	[illegible]	[illegible]	[illegible]	[illegible]	[illegible]	[illegible]	[illegible]	[illegible]
328-	0.267	0.384	3.130	0.174	0.454	1.447	0.269	0.701	1.080	0.317	0.826
333-	0.051	0.173	[illegible]	[illegible]	[illegible]	[illegible]	[illegible]	[illegible]	[illegible]	[illegible]	[illegible]
334-	0.030	0.079	[illegible]	[illegible]	[illegible]	[illegible]	[illegible]	[illegible]	[illegible]	[illegible]	[illegible]
335-	0.048	0.170	[illegible]	[illegible]	[illegible]	[illegible]	[illegible]	[illegible]	[illegible]	[illegible]	[illegible]

336-	0.058	0.175	[illegible]	[illegible]	[illegible]	[illegible]	[illegible]	[illegible]	[illegible]	[illegible]	[illegible]
336A	0.069	0.231	[illegible]	[illegible]	[illegible]	[illegible]	[illegible]	[illegible]	[illegible]	[illegible]	[illegible]
337-	0.084	0.221	[illegible]	[illegible]	[illegible]	[illegible]	[illegible]	[illegible]	[illegible]	[illegible]	[illegible]
338-	0.066	0.269	[illegible]	[illegible]	[illegible]	[illegible]	[illegible]	[illegible]	[illegible]	[illegible]	[illegible]
4001A	0.099	0.277	[illegible]	[illegible]	[illegible]	[illegible]	[illegible]	[illegible]	[illegible]	[illegible]	[illegible]
4001B	0.135	0.262	[illegible]	[illegible]	[illegible]	[illegible]	[illegible]	[illegible]	[illegible]	[illegible]	[illegible]
4001C	0.114	0.351	[illegible]	[illegible]	[illegible]	[illegible]	[illegible]	[illegible]	[illegible]	[illegible]	[illegible]
4001D	0.102	0.264	[illegible]	[illegible]	[illegible]	[illegible]	[illegible]	[illegible]	[illegible]	[illegible]	[illegible]
4002B	0.493	0.716	2.921	0.337	0.470	1.350	0.520	0.726	1.008	0.613	0.856
4002D	1.270	0.574	[illegible]	[illegible]	[illegible]	[illegible]	[illegible]	[illegible]	[illegible]	[illegible]	[illegible]
4002E	1.270	0.518	[illegible]	[illegible]	[illegible]	[illegible]	[illegible]	[illegible]	[illegible]	[illegible]	[illegible]
4003A	0.104	0.218	[illegible]	[illegible]	[illegible]	[illegible]	[illegible]	[illegible]	[illegible]	[illegible]	[illegible]
4003B	0.089	0.231	[illegible]	[illegible]	[illegible]	[illegible]	[illegible]	[illegible]	[illegible]	[illegible]	[illegible]
4003C	0.081	0.224	[illegible]	[illegible]	[illegible]	[illegible]	[illegible]	[illegible]	[illegible]	[illegible]	[illegible]
4003D	0.084	0.257	[illegible]	[illegible]	[illegible]	[illegible]	[illegible]	[illegible]	[illegible]	[illegible]	[illegible]
4004A	0.315	0.638	[illegible]	[illegible]	[illegible]	[illegible]	[illegible]	[illegible]	[illegible]	[illegible]	[illegible]
4004B	0.663	0.511	[illegible]	[illegible]	[illegible]	[illegible]	[illegible]	[illegible]	[illegible]	[illegible]	[illegible]
4101A	0.074	0.165	[illegible]	[illegible]	[illegible]	[illegible]	[illegible]	[illegible]	[illegible]	[illegible]	[illegible]
4101B	0.343	0.188	[illegible]	[illegible]	[illegible]	[illegible]	[illegible]	[illegible]	[illegible]	[illegible]	[illegible]
4101C	0.104	0.315	[illegible]	[illegible]	[illegible]	[illegible]	[illegible]	[illegible]	[illegible]	[illegible]	[illegible]
4102A	0.104	0.224	[illegible]	[illegible]	[illegible]	[illegible]	[illegible]	[illegible]	[illegible]	[illegible]	[illegible]
4102C	0.117	0.279	[illegible]	[illegible]	[illegible]	[illegible]	[illegible]	[illegible]	[illegible]	[illegible]	[illegible]
4102C1	0.089	0.333	[illegible]	[illegible]	[illegible]	[illegible]	[illegible]	[illegible]	[illegible]	[illegible]	[illegible]
4103A	0.015	0.107	0.000	[illegible]	[illegible]	[illegible]	[illegible]	[illegible]	[illegible]	[illegible]	[illegible]
4103B	0.170	0.340	0.373	0.458	1.546	[illegible]	[illegible]	[illegible]	[illegible]	[illegible]	[illegible]
4103C	0.104	0.218	0.108	0.640	2.929	0.050	0.988	4.523	0.037	1.165	[illegible]
4103D	0.135	0.300	0.074	1.089	3.560	0.034	1.680	5.506	0.026	1.946	[illegible]
4104A	0.211	0.295	3.764	0.122	0.413	1.740	0.188	0.638	1.299	0.222	0.752
4104B	0.124	0.345	0.018	2.550	7.382	0.008	3.938	11.401	0.006	4.644	[illegible]
4104C	0.170	0.386	0.065	1.455	3.794	[illegible]	2.262	5.859	0.023	2.667	[illegible]
4104D	0.130	0.315	0.042	1.502	4.760	[illegible]	2.319	7.364	0.014	2.736	[illegible]
4105A	0.292	0.518	0.808	0.470	0.907	0.374	0.726	1.401	0.279	0.856	[illegible]
4105A1	0.229	0.320	3.723	0.133	0.415	1.721	0.205	0.641	1.284	0.242	0.756
4105B	0.178	0.442	0.036	2.267	5.130	0.017	3.501	7.922	0.013	4.129	[illegible]
4106A	0.099	0.295	0.011	2.733	9.277	0.005	4.221	14.326	0.004	4.978	[illegible]
4106A1	0.325	0.333	28.102	0.049	0.148	12.992	0.076	0.228	9.696	0.089	0.269
4106B	0.112	0.267	0.047	1.196	4.483	0.022	1.847	6.924	0.016	2.178	[illegible]
4106B1	0.325	0.485	2.467	0.249	0.513	1.140	0.384	0.792	0.851	0.453	[illegible]
4106C	0.231	0.561	0.042	2.667	4.750	0.019	4.118	7.336	0.015	4.856	[illegible]
4106D	0.406	0.612	2.322	0.324	0.529	1.074	0.500	0.816	0.801	0.589	[illegible]
4107A	0.307	0.696	0.066	2.624	3.771	0.031	4.053	5.823	0.023	4.779	[illegible]
4107B	0.409	0.668	1.376	0.462	0.691	0.636	0.713	1.067	0.475	0.841	1.258
4107C	0.470	0.561	10.362	0.138	0.246	4.790	0.213	0.380	3.575	0.251	0.448
4107D	0.765	0.445	1079.677	0.010	0.023	499.161	0.016	0.035	372.511	0.018	0.042
4108A	0.544	1.031	0.524	1.168	1.132	0.242	1.803	1.749	0.181	2.127	[illegible]
4108A1	0.815	0.538	474.367	0.019	0.035	219.311	0.029	0.054	163.668	0.034	0.063
4108B	0.638	0.683	20.873	0.117	0.172	9.650	0.181	0.265	7.202	0.214	0.313
4109A	0.025	0.140	0.000	9.861	70.589	0.000	15.229	109.015	0.000	17.959	[illegible]
4109B	0.043	0.188	0.001	6.130	32.613	0.000	9.467	50.366	0.000	11.164	[illegible]
4109C	0.053	0.191	0.003	3.233	16.970	0.002	4.992	26.207	0.001	5.887	[illegible]
4110A	0.114	0.193	1.110	0.149	0.771	0.513	0.230	1.191	0.383	0.271	[illegible]
4110B	0.081	0.180	0.075	0.636	3.525	[illegible]	0.982	5.444	[illegible]	1.158	[illegible]
4110C	0.046	0.234	0.000	12.949	65.412	[illegible]	[illegible]	[illegible]	[illegible]	23.581	[illegible]
4110D	0.076	0.302	0.002	7.253	23.997	[illegible]	11.202	37.060	0.001	13.210	[illegible]
4111A	0.061	0.310	0.000	16.865	54.424	[illegible]	26.045	84.049	[illegible]	30.713	[illegible]
4111B	0.160	0.340	0.099	1.044	3.066	[illegible]	1.612	4.736	0.034	1.901	[illegible]
4111C	0.130	0.312	0.044	1.450	4.643	[illegible]	2.240	7.170	0.015	2.642	[illegible]
4111D	0.132	0.257	0.450	0.314	1.224	0.208	0.485	1.890	0.155	0.572	[illegible]

4112A	0.122	0.270									
4112B	0.231	0.507	5.101	[illegible]	[illegible]	2.400	[illegible]	[illegible]	1.791	0.196	0.638
4112C	0.076	0.200									
4112D	0.150	0.343									
4113A	0.176	0.380									
4113B	0.190	[illegible]	0.372	[illegible]	[illegible]						
4113C	0.400	[illegible]				[illegible]	[illegible]	[illegible]	[illegible]	0.148	0.328
4113D	0.130	[illegible]									
4114A	[illegible]	[illegible]									
4114B	0.345	[illegible]									
4114C	0.333	[illegible]				4.889	[illegible]	[illegible]	3.648	0.176	0.443
4114D	0.241	[illegible]									
4115A	[illegible]	[illegible]	[illegible]	[illegible]	[illegible]	[illegible]	[illegible]	[illegible]	[illegible]	[illegible]	0.723
4115B	0.100	[illegible]									
4115C	0.495	[illegible]									
4115D	0.427	[illegible]				[illegible]	[illegible]	0.312	[illegible]	0.176	0.367
4116A	0.409	[illegible]				[illegible]	[illegible]	[illegible]	[illegible]	[illegible]	[illegible]
4116B	0.312	[illegible]	[illegible]	[illegible]	[illegible]						
4116C	[illegible]	[illegible]									
4116D	0.688	[illegible]									
4117A	0.452	[illegible]				[illegible]	[illegible]	[illegible]	[illegible]	0.190	0.372
4117B	1.270	[illegible]									
4117C	1.356	0.462									
4117D	1.212	0.447									

Test No.	p	d	V3-14	D3-14	D3-14/d	V9-13	D9-13	D9-13/d	V6-13	D6-13
No.	(cm)	(cm)								
EHAB	0.615	0.734	[illegible]	[illegible]	[illegible]	[illegible]	[illegible]	[illegible]	[illegible]	[illegible]
EHPB	0.495	0.650	[illegible]	[illegible]	[illegible]	[illegible]	[illegible]	[illegible]	[illegible]	[illegible]
EHPC	0.386	0.599	[illegible]	[illegible]	[illegible]	[illegible]	[illegible]	[illegible]	[illegible]	[illegible]
EHRP1	0.117	0.244	[illegible]	[illegible]	[illegible]	[illegible]	[illegible]	[illegible]	1.352	0.142
EHRP2	0.371	0.632	[illegible]	[illegible]	[illegible]	[illegible]	[illegible]	[illegible]	[illegible]	[illegible]
EHRP3	0.165	0.368	[illegible]	[illegible]	[illegible]	[illegible]	[illegible]	[illegible]	2.216	0.150
EHRP4	0.216	0.371	[illegible]	[illegible]	[illegible]	[illegible]	[illegible]	[illegible]	[illegible]	[illegible]
EHRP5	0.330	0.546	[illegible]	[illegible]	[illegible]	[illegible]	[illegible]	[illegible]	[illegible]	[illegible]
EHRP6	0.114	0.267	[illegible]	[illegible]	[illegible]	[illegible]	[illegible]	[illegible]	3.175	0.084
EHRP7	0.323	0.488	[illegible]	[illegible]	[illegible]	[illegible]	[illegible]	[illegible]	[illegible]	[illegible]
EHRP8	0.137	0.279	[illegible]	[illegible]	[illegible]	[illegible]	[illegible]	[illegible]	1.136	0.184
EHRP9	0.244	0.676	[illegible]	[illegible]	[illegible]	1.841	0.291	0.430	[illegible]	[illegible]
EHSS4C	0.188	0.353	[illegible]	[illegible]	[illegible]	[illegible]	[illegible]	[illegible]	[illegible]	[illegible]
001B	0.117	0.257	[illegible]	[illegible]	[illegible]	[illegible]	[illegible]	[illegible]	1.975	0.114
002B	0.084	0.287	[illegible]	[illegible]	[illegible]	7.931	0.043	0.151	[illegible]	[illegible]
201A	0.071	0.180	[illegible]	[illegible]	[illegible]	0.999	0.120	0.666	5.693	0.038
205A	0.122	0.224	[illegible]	[illegible]	[illegible]	[illegible]	[illegible]	[illegible]	[illegible]	[illegible]
205C	0.084	0.180	[illegible]	[illegible]	[illegible]	[illegible]	[illegible]	[illegible]	1.701	0.089
205D	0.074	0.234	[illegible]	[illegible]	[illegible]	4.683	0.052	0.221	[illegible]	[illegible]
205E	0.058	0.226	[illegible]	[illegible]	[illegible]	[illegible]	[illegible]	[illegible]	[illegible]	[illegible]
206E	0.030	0.178	[illegible]	[illegible]	[illegible]	[illegible]	[illegible]	[illegible]	[illegible]	[illegible]
206F	0.094	0.155	0.148	0.375	0.756	[illegible]	[illegible]	[illegible]	[illegible]	[illegible]
211B	0.147	0.267	[illegible]	[illegible]	[illegible]	[illegible]	[illegible]	[illegible]	[illegible]	[illegible]
211D	0.132	0.267	[illegible]	[illegible]	[illegible]	[illegible]	[illegible]	[illegible]	1.067	0.183
212B	0.079	0.244	[illegible]	[illegible]	[illegible]	3.965	0.061	0.249	[illegible]	[illegible]
216A	0.097	0.284	[illegible]	[illegible]	[illegible]	2.819	0.090	0.317	[illegible]	[illegible]
216C	0.147	0.333	[illegible]	[illegible]	[illegible]	[illegible]	[illegible]	[illegible]	2.431	0.127
217A	0.091	0.249	[illegible]	[illegible]	[illegible]	1.630	0.117	0.469	9.593	0.036
217B	0.196	0.234	1.181	0.195	0.394	[illegible]	[illegible]	[illegible]	[illegible]	[illegible]
217C	0.091	0.193	[illegible]	[illegible]	[illegible]	[illegible]	[illegible]	[illegible]	1.479	0.105
217D	0.074	0.224	[illegible]	[illegible]	[illegible]	3.446	0.061	0.275	[illegible]	[illegible]
217E	0.046	0.180	[illegible]	[illegible]	[illegible]	[illegible]	[illegible]	[illegible]	[illegible]	[illegible]
218A	0.102	0.292	[illegible]	[illegible]	[illegible]	2.375	0.105	0.358	[illegible]	[illegible]
218C	0.160	0.307	[illegible]	[illegible]	[illegible]	[illegible]	[illegible]	[illegible]	[illegible]	[illegible]
221B	0.051	0.193	[illegible]	[illegible]	[illegible]	[illegible]	[illegible]	[illegible]	[illegible]	[illegible]
221C	0.030	0.081	[illegible]	[illegible]	[illegible]	1.414	0.042	0.519	8.243	0.013
226A	0.010	0.157	[illegible]	[illegible]	[illegible]	[illegible]	[illegible]	[illegible]	[illegible]	[illegible]
226B	0.069	0.249	[illegible]	[illegible]	[illegible]	[illegible]	[illegible]	[illegible]	[illegible]	[illegible]
227A	0.259	0.216	[illegible]	[illegible]	[illegible]	[illegible]	[illegible]	[illegible]	[illegible]	[illegible]
227B	0.069	0.208	[illegible]	[illegible]	[illegible]	3.467	0.057	0.274	[illegible]	[illegible]
230B	0.097	0.218	[illegible]	[illegible]	[illegible]	[illegible]	[illegible]	[illegible]	2.467	0.083
230C	0.076	0.229	[illegible]	[illegible]	[illegible]	3.185	0.066	0.291	[illegible]	[illegible]
230D	0.114	0.224	[illegible]	[illegible]	[illegible]	[illegible]	[illegible]	[illegible]	[illegible]	[illegible]
230E	0.109	0.284	[illegible]	[illegible]	[illegible]	1.202	0.166	0.583	6.934	0.052
301-	0.066	0.218	[illegible]	[illegible]	[illegible]	6.246	0.039	0.180	[illegible]	[illegible]
303-	0.198	0.257	0.703	0.280	0.564	[illegible]	[illegible]	[illegible]	[illegible]	[illegible]
303A	0.041	0.333	[illegible]	[illegible]	[illegible]	[illegible]	[illegible]	[illegible]	[illegible]	[illegible]
303B	0.191	0.188	4.059	0.084	0.168	[illegible]	[illegible]	[illegible]	[illegible]	[illegible]
319-	0.074	0.213	[illegible]	[illegible]	[illegible]	2.501	0.074	0.346	[illegible]	[illegible]
321-	0.180	0.231	0.751	0.244	0.491	[illegible]	[illegible]	[illegible]	[illegible]	[illegible]
324-	0.064	0.224	[illegible]	[illegible]	[illegible]	9.592	0.030	0.132	[illegible]	[illegible]
325-	0.066	0.224	[illegible]	[illegible]	[illegible]	7.319	0.036	0.160	[illegible]	[illegible]
326-	0.267	0.384	0.357	0.591	1.192	[illegible]	[illegible]	[illegible]	[illegible]	[illegible]
333-	0.051	0.173	[illegible]	[illegible]	[illegible]	7.551	0.027	0.157	[illegible]	[illegible]
334-	0.030	0.079	[illegible]	[illegible]	[illegible]	1.136	0.048	0.608	6.527	0.015
335-	0.048	0.170	[illegible]	[illegible]	[illegible]	9.711	0.022	0.131	[illegible]	[illegible]

Test No.	p	d	V3-14	D3-14	D3-14/d	V9-13	D9-13	D9-13/d	V6-13	D6-13	D6-13/d
No.	(cm)	(cm)									
EHAB	0.615	0.734									
EHPB	0.495	0.650									
EHPC	0.386	0.509									
EHRP1	0.117	0.244							1.352	0.142	0.581
EHRP2	0.371	0.632									
EHRP3	0.165	0.366							2.216	0.150	0.409
EHRP4	0.216	0.371									
EHRP5	0.330	0.546									
EHRP6	0.114	0.267							3.175	0.084	0.316
EHRP7	0.323	0.486									
EHRP8	0.137	0.279							1.136	0.184	0.658
EHRP9	0.244	0.676				1.841	0.291	0.430			
EHS84C	0.158	0.353									
001B	0.117	0.257							1.975	0.114	0.444
002B	0.084	0.287				7.931	0.043	0.151			
201A	0.071	0.180				0.899	[illegible]	0.666	5.693	0.038	0.209
205A	0.122	0.224									
205C	0.084	0.180							1.701	0.089	0.493
205D	0.074	0.234				4.683	[illegible]	0.221			
205E	0.058	0.226									
206E	0.030	0.178									
206F	0.094	0.155	0.144	[illegible]	[illegible]						
211B	0.147	0.267									
211D	0.132	0.267							1.067	0.183	0.688
212B	0.079	0.244				3.966	0.061	0.249			
216A	0.097	0.284				2.818	0.090	0.317			
216C	0.147	0.333							2.431	0.127	0.383
217A	0.091	0.249				1.630	0.117	0.469	9.593	0.036	0.144
217B	0.196	0.234	1.181	0.195	0.394						
217C	0.091	0.193							1.479	0.105	0.545
217D	0.074	0.224				3.446	0.061	0.275			
217E	0.046	0.180									
218A	0.102	0.292				2.375	0.105	0.358			
218C	0.160	0.307									
221B	0.051	0.193									
221C	0.030	0.081				1.414	0.042	0.519	8.243	0.013	0.160
226A	0.010	0.157									
226B	0.069	0.249									
227A	0.259	0.216									
227B	0.069	0.208				3.467	0.057	0.274			
230B	0.097	0.218							2.467	0.083	0.379
230C	0.076	0.229				3.185	0.066	0.291			
230D	0.114	0.224									
230E	0.109	0.284				1.202	0.166	0.583	6.934	0.052	0.181
301-	0.066	0.218				6.246	0.039	0.180			
303-	0.198	0.257	0.703	0.280	0.564						
303A	0.041	0.333									
303B	0.191	0.188	4.059	0.084	0.168						
319-	0.074	0.213				2.501	0.074	0.346			
321-	0.180	0.231	0.751	0.244	0.491						
324-	0.084	0.224				9.592	0.030	0.132			
325-	0.066	0.224				7.319	0.036	0.160			
326-	0.267	0.384	0.357	0.591	1.192						
333-	0.051	0.173				7.551	0.027	0.157			
334-	0.030	0.079				1.136	0.048	0.608	6.527	0.015	0.189
335-	0.048	0.170				9.711	0.022	0.131			

338-	0.058	0.175	[illegible]	[illegible]	[illegible]	3.185	0.051	0.291	[illegible]	[illegible]	[illegible]
336A	0.069	0.231	[illegible]	[illegible]	[illegible]	7.109	0.038	0.164	[illegible]	[illegible]	[illegible]
337-	0.084	0.221	[illegible]	[illegible]	[illegible]	1.307	0.121	0.550	7.579	0.038	0.170
338-	0.066	0.269	[illegible]	[illegible]	[illegible]	[illegible]	[illegible]	[illegible]	[illegible]	[illegible]	[illegible]
4001A	0.099	0.277	[illegible]	[illegible]	[illegible]	1.954	0.114	0.412	[illegible]	[illegible]	[illegible]
4001B	0.135	0.262	[illegible]	[illegible]	[illegible]	[illegible]	[illegible]	[illegible]	[illegible]	[illegible]	[illegible]
4001C	0.114	0.351	[illegible]	[illegible]	[illegible]	3.707	0.091	0.261	[illegible]	[illegible]	[illegible]
4001D	0.102	0.264	[illegible]	[illegible]	[illegible]	1.187	0.155	0.589	6.843	0.048	0.183
4002B	0.493	0.716	0.333	1.144	2.307	[illegible]	[illegible]	[illegible]	[illegible]	[illegible]	[illegible]
4002D	1.270	0.574	[illegible]	[illegible]	[illegible]	[illegible]	[illegible]	[illegible]	[illegible]	[illegible]	[illegible]
4002E	1.270	0.518	[illegible]	[illegible]	[illegible]	[illegible]	[illegible]	[illegible]	[illegible]	[illegible]	[illegible]
4003A	0.104	0.218	[illegible]	[illegible]	[illegible]	[illegible]	[illegible]	[illegible]	1.411	0.123	0.563
4003B	0.089	0.231	[illegible]	[illegible]	[illegible]	1.187	0.136	0.589	6.843	0.042	0.183
4003C	0.081	0.224	[illegible]	[illegible]	[illegible]	1.748	0.100	0.446	[illegible]	[illegible]	[illegible]
4003D	0.084	0.257	[illegible]	[illegible]	[illegible]	3.656	0.068	0.263	[illegible]	[illegible]	[illegible]
4004A	0.315	0.638	[illegible]	[illegible]	[illegible]	[illegible]	[illegible]	[illegible]	1.086	0.433	0.679
4004B	0.663	0.511	[illegible]	[illegible]	[illegible]	[illegible]	[illegible]	[illegible]	[illegible]	[illegible]	[illegible]
4101A	0.074	0.165	[illegible]	[illegible]	[illegible]	[illegible]	[illegible]	[illegible]	2.298	0.066	0.398
4101B	0.343	0.188	[illegible]	[illegible]	[illegible]	[illegible]	[illegible]	[illegible]	[illegible]	[illegible]	[illegible]
4101C	0.104	0.315	[illegible]	[illegible]	[illegible]	3.368	0.088	0.279	[illegible]	[illegible]	[illegible]
4102A	0.104	0.224	[illegible]	[illegible]	[illegible]	[illegible]	[illegible]	[illegible]	1.671	0.112	0.500
4102C	0.117	0.279	[illegible]	[illegible]	[illegible]	0.667	0.248	0.889	3.699	0.079	0.284
4102C1	0.089	0.333	[illegible]	[illegible]	[illegible]	[illegible]	[illegible]	[illegible]	[illegible]	[illegible]	[illegible]
4103A	0.015	0.107	[illegible]	[illegible]	[illegible]	[illegible]	[illegible]	[illegible]	[illegible]	[illegible]	[illegible]
4103B	0.170	0.340	[illegible]	[illegible]	[illegible]	[illegible]	[illegible]	[illegible]	[illegible]	[illegible]	[illegible]
4103C	0.104	0.218	[illegible]	[illegible]	[illegible]	[illegible]	[illegible]	[illegible]	1.411	0.123	0.563
4103D	0.135	0.300	[illegible]	[illegible]	[illegible]	[illegible]	[illegible]	[illegible]	2.187	0.124	0.412
4104A	0.211	0.295	0.429	0.413	0.833	[illegible]	[illegible]	[illegible]	[illegible]	[illegible]	[illegible]
4104B	0.124	0.345	[illegible]	[illegible]	[illegible]	1.863	0.147	0.426	[illegible]	[illegible]	[illegible]
4104C	0.170	0.386	[illegible]	[illegible]	[illegible]	[illegible]	[illegible]	[illegible]	2.512	0.144	0.374
4104D	0.130	0.315	[illegible]	[illegible]	[illegible]	0.748	0.258	0.819	4.180	0.082	0.260
4105A	0.292	0.518	[illegible]	[illegible]	[illegible]	[illegible]	[illegible]	[illegible]	[illegible]	[illegible]	[illegible]
4105A1	0.229	0.320	0.425	0.451	0.910	[illegible]	[illegible]	[illegible]	[illegible]	[illegible]	[illegible]
4105B	0.178	0.442	[illegible]	[illegible]	[illegible]	0.871	0.325	0.735	4.917	0.102	0.232
4106A	0.099	0.295	[illegible]	[illegible]	[illegible]	3.002	0.089	0.303	[illegible]	[illegible]	[illegible]
4106A1	0.325	0.333	3.206	0.167	0.336	[illegible]	[illegible]	[illegible]	[illegible]	[illegible]	[illegible]
4106B	0.112	0.267	[illegible]	[illegible]	[illegible]	0.657	0.240	0.898	3.643	0.076	0.287
4106B1	0.325	0.485	0.281	0.845	1.704	[illegible]	[illegible]	[illegible]	[illegible]	[illegible]	[illegible]
4106C	0.231	0.561	[illegible]	[illegible]	[illegible]	0.742	0.462	0.824	4.144	0.147	0.262
4106D	0.406	0.612	0.265	1.099	2.217	[illegible]	[illegible]	[illegible]	[illegible]	[illegible]	[illegible]
4107A	0.307	0.696	[illegible]	[illegible]	[illegible]	[illegible]	[illegible]	[illegible]	2.478	0.263	0.377
4107B	0.409	0.668	[illegible]	[illegible]	[illegible]	[illegible]	[illegible]	[illegible]	[illegible]	[illegible]	[illegible]
4107C	0.470	0.561	1.182	0.469	0.946	[illegible]	[illegible]	[illegible]	[illegible]	[illegible]	[illegible]
4107D	0.765	0.445	[illegible]	[illegible]	[illegible]	[illegible]	[illegible]	[illegible]	[illegible]	[illegible]	[illegible]
4108A	0.544	1.031	[illegible]	[illegible]	[illegible]	[illegible]	[illegible]	[illegible]	[illegible]	[illegible]	[illegible]
4108A1	0.815	0.538	[illegible]	[illegible]	[illegible]	[illegible]	[illegible]	[illegible]	[illegible]	[illegible]	[illegible]
4108B	0.638	0.683	2.381	0.399	0.805	[illegible]	[illegible]	[illegible]	[illegible]	[illegible]	[illegible]
4109A	0.025	0.140	[illegible]	[illegible]	[illegible]	[illegible]	[illegible]	[illegible]	[illegible]	[illegible]	[illegible]
4109B	0.043	0.188	[illegible]	[illegible]	[illegible]	[illegible]	[illegible]	[illegible]	[illegible]	[illegible]	[illegible]
4109C	0.053	0.191	[illegible]	[illegible]	[illegible]	[illegible]	[illegible]	[illegible]	[illegible]	[illegible]	[illegible]
4110A	0.114	0.193	0.127	0.506	1.020	[illegible]	[illegible]	[illegible]	[illegible]	[illegible]	[illegible]
4110B	0.081	0.180	[illegible]	[illegible]	[illegible]	[illegible]	[illegible]	[illegible]	2.133	0.076	0.420
4110C	0.046	0.234	[illegible]	[illegible]	[illegible]	[illegible]	[illegible]	[illegible]	[illegible]	[illegible]	[illegible]
4110D	0.076	0.302	[illegible]	[illegible]	[illegible]	[illegible]	[illegible]	[illegible]	[illegible]	[illegible]	[illegible]
4111A	0.061	0.310	[illegible]	[illegible]	[illegible]	[illegible]	[illegible]	[illegible]	[illegible]	[illegible]	[illegible]
4111B	0.160	0.340	[illegible]	[illegible]	[illegible]	[illegible]	[illegible]	[illegible]	1.563	0.178	0.524
4111C	0.130	0.312	[illegible]	[illegible]	[illegible]	[illegible]	[illegible]	[illegible]	3.938	0.085	0.271
4111D	0.132	0.257	[illegible]	[illegible]	[illegible]	[illegible]	[illegible]	[illegible]	[illegible]	[illegible]	[illegible]

[illegible]	0.122	[illegible]							2.706	0.099	0.356
[illegible]	0.221	[illegible]	[illegible]	[illegible]	[illegible]						
[illegible]	0.070	[illegible]									
[illegible]	0.140	[illegible]							2.674	0.123	0.357
[illegible]	0.170	[illegible]							[illegible]	0.181	0.470
[illegible]	[illegible]	[illegible]									
4113C	0.400	[illegible]	2.174	0.222	[illegible]						
[illegible]	[illegible]	[illegible]				[illegible]	[illegible]	[illegible]			
[illegible]	[illegible]	[illegible]									
[illegible]	[illegible]	[illegible]									
4114C	0.333	[illegible]	[illegible]	[illegible]	[illegible]						
4114D	0.241	[illegible]									
[illegible]	0.363	[illegible]	[illegible]	[illegible]	[illegible]						
[illegible]	0.160	[illegible]							[illegible]	[illegible]	[illegible]
4115C	0.495	0.368									
[illegible]	0.427	0.489	[illegible]	[illegible]	[illegible]						
4116A	0.409	0.445	[illegible]	[illegible]	[illegible]						
[illegible]	0.312	[illegible]									
4116C	0.384	0.742									
4116D	0.688	0.564									
4117A	0.452	0.511	[illegible]	[illegible]	[illegible]						
4117B	1.270	0.404									
4117C	1.358	[illegible]									
4117D	1.212	0.447									

APPENDIX F

CALCULATED RICOCHET PARTICLE MAX—MIN COMBINATIONS

Table F-1 Calculated Ricochet Particle Max-Min Combinations
Phase B NASA/MSFC Test Series

Test No.	V_p (km/s)	θ_p (deg)	d_p (cm)	t_b (cm)	V_{max} (km/s	d_{min} (cm)	V_{min} (km/s)	d_{max} (cm)
001B	6.56	45	0.795	0.203	5.394	0.082	2.833	0.118
002B	6.51	45	0.795	0.160	7.931	0.043	7.931	0.043
201A	4.33	45	0.635	0.102	2.130	0.093	0.999	0.120
205A	4.20	45	0.635	0.160	1.306	0.153	1.306	0.153
205C	5.30	45	0.635	0.160	6.149	0.054	3.229	0.077
205D	6.42	45	0.635	0.160	4.683	0.052	4.683	0.052
206F	6.42	45	0.475	0.160	2.590	0.075	1.296	0.110
211B	5.88	45	0.889	0.160	1.416	0.175	1.416	0.175
211D	6.84	45	0.889	0.160	9.261	0.065	4.863	0.093
212B	6.38	45	0.762	0.160	3.965	0.061	3.965	0.061
216A	6.10	45	0.889	0.203	2.819	0.090	0.807	0.240
216C	6.96	45	0.795	0.203	4.495	0.117	2.360	0.168
217A	6.65	45	0.795	0.102	1.630	0.117	1.348	0.162
217B	7.10	45	0.795	0.102	4.785	0.089	1.181	0.195
217C	6.05	45	0.635	0.102	6.950	0.054	3.649	0.078
217D	6.47	45	0.635	0.102	3.446	0.061	3.446	0.061
218A	5.82	45	0.889	0.102	2.375	0.105	0.947	0.227
218C	6.88	45	0.889	0.102	0.967	0.245	0.967	0.245
221C	4.62	45	0.475	0.102	1.539	0.049	0.808	0.071
227B	7.25	45	0.635	0.081	3.467	0.057	0.665	0.194
230B	3.23	45	0.475	0.160	4.437	0.077	2.330	0.111
230C	5.16	45	0.635	0.160	3.185	0.066	0.720	0.204
230D	5.51	45	0.635	0.160	0.861	0.189	0.861	0.189
230E	6.62	45	0.635	0.160	1.792	0.160	1.202	0.166
301-	2.95	45	0.635	0.160	6.246	0.039	6.246	0.039
303-	4.59	45	0.795	0.160	6.160	0.082	2.125	0.150
303B	4.34	45	0.795	0.160	4.059	0.084	4.059	0.084
319-	2.93	45	0.795	0.102	2.501	0.074	0.903	0.170
321-	2.97	45	0.795	0.203	6.580	0.072	2.270	0.131
324-	4.05	45	0.795	0.102	9.592	0.030	9.592	0.030
325-	4.14	45	0.795	0.160	7.319	0.036	7.319	0.036
326-	4.22	45	0.795	0.203	6.255	0.118	1.080	0.317
333-	2.88	45	0.475	0.102	7.551	0.027	7.551	0.027
334-	3.61	45	0.475	0.102	1.889	0.043	1.136	0.048
335-	4.07	45	0.635	0.102	9.711	0.022	9.711	0.022
336-	4.47	45	0.635	0.102	3.185	0.051	3.185	0.051
336A	5.70	45	0.635	0.102	7.109	0.038	7.109	0.038
337-	6.81	45	0.795	0.102	1.657	0.129	1.307	0.121

Table F-2 Calculated Ricochet Particle Max-Min Combinations
Phase C/D NASA/MSFC Test Series

Test No.	V_p (km/s)	θ_p (deg)	d_p (cm)	t_b (cm)	V_{max} (km/s	d_{min} (cm)	V_{min} (km/s)	d_{max} (cm)
4001A	3.15	45	0.795	0.203	1.954	0.114	1.137	0.196
4001C	6.12	45	0.795	0.203	3.707	0.091	3.707	0.091
4001D	6.71	45	0.795	0.203	1.813	0.147	1.187	0.155
4002B	3.97	75	0.795	0.203	5.836	0.228	2.921	0.337
4003A	3.43	45	0.795	0.160	7.244	0.060	3.804	0.086
4003B	6.29	45	0.795	0.203	1.813	0.129	0.952	0.185
4003C	3.18	45	0.795	0.203	1.748	0.100	1.262	0.150
4003D	6.22	45	0.795	0.203	3.656	0.068	3.656	0.068
4004A	3.19	75	0.795	0.203	9.115	0.156	4.787	0.224
4101A	3.14	45	0.635	0.127	4.723	0.056	2.298	0.066
4101C	6.14	45	0.635	0.127	3.368	0.088	3.368	0.088
4102A	2.95	45	0.795	0.127	6.246	0.066	3.280	0.095
4102C	6.24	45	0.795	0.127	3.699	0.079	1.633	0.170
4103C	5.88	60	0.475	0.127	7.244	0.060	3.804	0.086
4103D	7.37	60	0.475	0.127	4.931	0.100	2.187	0.124
4104A	7.23	60	0.635	0.127	7.521	0.082	3.764	0.122
4104B	4.19	60	0.635	0.127	1.863	0.147	1.189	0.239
4104C	6.12	60	0.635	0.127	4.368	0.137	2.294	0.197
4104D	7.52	60	0.635	0.127	4.180	0.082	1.467	0.202
4105A	2.92	60	0.795	0.127	1.615	0.318	1.615	0.318
4105A1	2.98	60	0.795	0.127	7.437	0.090	3.723	0.133
4105B	4.02	60	0.795	0.127	4.917	0.102	1.272	0.305
4106A	3.05	60	0.475	0.127	3.002	0.089	0.761	0.256
4106A1	3.10	75	0.475	0.127	9.696	0.089	3.206	0.167
4106B	4.12	60	0.475	0.127	3.643	0.076	1.655	0.161
4106B1	3.99	75	0.475	0.127	4.929	0.168	2.467	0.249
4106C	5.95	75	0.475	0.127	2.815	0.250	1.478	0.359
4106D	7.56	75	0.475	0.127	4.639	0.219	2.322	0.324
4107A	3.05	75	0.475	0.127	4.420	0.246	2.321	0.354
4107B	4.11	75	0.635	0.127	2.749	0.313	1.376	0.462
4107C	6.20	75	0.635	0.127	4.790	0.213	1.182	0.469
4108A	3.12	75	0.795	0.127	1.047	0.791	1.047	0.791
4108B	3.97	75	0.795	0.127	9.650	0.181	7.202	0.214
4110A	3.25	45	0.635	0.203	2.217	0.101	1.110	0.149
4110B	4.00	45	0.635	0.203	5.042	0.060	2.648	0.086
4111B	3.94	45	0.795	0.203	6.622	0.098	3.477	0.141
4111C	5.97	45	0.795	0.203	2.944	0.136	1.546	0.195
4111D	6.81	45	0.795	0.203	0.900	0.213	0.900	0.213
4112A	3.33	60	0.475	0.203	4.093	0.103	2.149	0.148

4112B	4.05	60	0.475	0.203	5.191	0.108	2.400	0.166
4112D	7.50	60	0.475	0.203	4.134	0.125	2.171	0.180
4113A	2.97	60	0.635	0.203	5.795	0.119	3.043	0.171
4113B	3.77	60	0.635	0.203	1.742	0.203	0.872	0.299
4113C	6.30	60	0.635	0.203	8.810	0.124	6.574	0.146
4113D	7.12	60	0.635	0.203	4.527	0.092	4.527	0.092
4114A	3.13	60	0.795	0.203	1.382	0.286	1.382	0.286
4114C	5.92	60	0.795	0.203	4.889	0.149	3.648	0.176
4115A	3.13	75	0.475	0.203	8.112	0.131	4.060	0.194
4115B	4.08	75	0.475	0.203	8.463	0.083	4.444	0.119
4115D	7.30	75	0.475	0.203	7.056	0.150	5.266	0.176
4116A	2.92	75	0.635	0.203	8.810	0.124	6.574	0.146
4116B	4.84	75	0.635	0.203	1.944	0.301	0.973	0.444
4117A	3.11	75	0.795	0.203	6.888	0.161	5.140	0.190

Table F-3 Calculated Ricochet Particle Max-Min Combinations NASA/MSFC EH Test Series

Test No.	V_p (km/s)	θ_p (deg)	d_p (cm)	t_b (cm)	V_{max} (km/s	d_{min} (cm)	V_{min} (km/s)	d_{max} (cm)
EHAB	6.91	75	0.795	0.160	4.819	0.278	3.596	0.328
EHPB	7.22	75	0.635	0.160	5.628	0.218	1.942	0.398
EHPC	7.58	75	0.475	0.160	3.828	0.237	1.916	0.349
EHRP1	6.87	60	0.795	0.160	7.520	0.066	3.949	0.094
EHRP2	6.80	65	0.795	0.160	2.097	0.340	1.050	0.502
EHRP3	6.78	45	0.795	0.160	4.876	0.124	2.216	0.150
EHRP4	7.65	60	0.635	0.160	1.989	0.205	0.995	0.303
EHRP5	7.51	65	0.635	0.160	2.531	0.266	1.267	0.394
EHRP6	7.57	45	0.635	0.160	3.556	0.105	1.868	0.152
EHRP7	7.98	60	0.475	0.160	4.549	0.176	1.053	0.402
EHRP8	7.34	45	0.475	0.160	8.766	0.069	4.603	0.100
EHRP9	7.29	65	0.475	0.160	1.841	0.291	1.202	0.465
EHSS4C	5.53	45	0.635	0.160	1.116	0.262	1.116	0.262

REPORT DOCUMENTATION PAGE

Form Approved
OMB No. 0704-0188

1. AGENCY USE ONLY *(Leave Blank)*

2. REPORT DATE
August 1999

3. REPORT TYPE AND DATES COVERED
Contractor Report (Final)

4. TITLE AND SUBTITLE
Characterizing Secondary Debris Impact Ejecta

5. FUNDING NUMBERS

6. AUTHORS
W.P. Schonberg

7. PERFORMING ORGANIZATION NAMES(S) AND ADDRESS(ES)
University of Alabama in Huntsville
Huntsville, AL 35899

8. PERFORMING ORGANIZATION REPORT NUMBER
M–934

9. SPONSORING/MONITORING AGENCY NAME(S) AND ADDRESS(ES)
National Aeronautics and Space Administration
Washington, DC 20546–0001

10. SPONSORING/MONITORING AGENCY REPORT NUMBER
NASA/CR—1999–209561

11. SUPPLEMENTARY NOTES
Prepared for NASA's Space Environments and Effects (SEE) Program
Technical Monitor: Greg Olsen

12a. DISTRIBUTION/AVAILABILITY STATEMENT
Unclassified-Unlimited
Subject Category 88
Standard Distribution

12b. DISTRIBUTION CODE

13. ABSTRACT *(Maximum 200 words)*

All spacecraft in low-Earth orbit are subject to high-speed impacts by meteoroids and orbital debris particles. These impacts can damage flight-critical systems, which can in turn lead to catastrophic failure of the spacecraft. Therefore, the design of a spacecraft for an Earth-orbiting mission must take into account the possibility of such impacts and their effects on the spacecraft structure and on all of its exposed subsystem components. In addition to threatening the operation of the spacecraft itself, on-orbit impacts also generate a significant amount of ricochet particles. These high-speed particles can destroy critical external spacecraft subsystems and also increase the contamination of the orbital environment.

This report presents a summary of the work performed towards the development of an empirical model that characterizes the secondary ejecta created by a high-speed impacta on a typical aerospace structural surface.

14. SUBJECT TERMS
hypervelocity impact, meteoroids, orbital debris

15. NUMBER OF PAGES
90

16. PRICE CODE
A05

17. SECURITY CLASSIFICATION OF REPORT	18. SECURITY CLASSIFICATION OF THIS PAGE	19. SECURITY CLASSIFICATION OF ABSTRACT	20. LIMITATION OF ABSTRACT
Unclassified	Unclassified	Unclassified	Unlimited

NSN 7540-01-280-5500

Standard Form 298 (Rev. 2-89)
Prescribed by ANSI Std. 239-18
298-102